INVESTIGATION OF THE EFFECT OF ATMOSPHERIC DUST ON THE DETERMINATION OF TOTAL OZONE FROM THE EARTH'S ULTRAVIOLET REFLECTIVITY MEASUREMENTS;

FINAL REPORT

(May 12, 1977)

Contract No. NAS5-23556

Prepared by

J. V. Dave

International Business Machines Corporation
Federal Systems Division
18100 Frederick Pike
Gaithersburg, Maryland 20760

For

National Aeronautics and Space Administration
Goddard Space Flight Center
Greenbelt, Maryland 20771

TABLE OF CONTENTS

		Page
	Abstract	1
	List of Figures	3
	List of Symbols	6
	List of Tables	11
I.	Introduction	14
	1.1 Background	14
	1.2 Algorithm for the Computations of Intensity	18
	1.3 Analysis of the Total-Ozone Estimation Procedure	21
	1.4 General Outline of this Report	26
II.	Aerosol Models	29
	2.1 Physical Characteristics	29
	2.2 Volume Cross-Sections	32
	2.3 Normalized Phase Function	41
III.	Atmospheric Models	46
	3.1 Height-Distribution Characteristics of Aerosols	46
	3.2 Total Aerosol Contents of Various Models	50
	3.3 Nomenclature	53
	3.4 Optical Thicknesses for the Models with 0.250 atm-cm Total Ozone	58
	3.5 Optical Thicknesses for the Models with 0.450 atm-cm Total Ozone	59
IV.	Discussion of Results	66
	4.1 General	66
	4.2 Physical Explanation	67
	4.3 *Deviations* Δ and Δ'	69
	4.4 Effect of the Stratospheric Aerosols	75
	4.5 Effect of the Tropospheric Aerosols	88
	4.6 Combined Effect	95
	4.7 Effect of a Change in the Size-Distribution Function	100

Page

V. Conclusion. 103

VI. References. 107

ABSTRACT

This final report for the NASA Contract No. NAS5-23556 contains the results of investigations on the effect of atmospheric aerosols on the value of total ozone, in an atmospheric column of the terrestrial atmosphere, estimated from the simulated measurements of the ultraviolet radiation back-scattered by the earth-atmosphere models. These investigations are carried out by making use of the simulated measurements in five (configuration of the BUV experiment on NIMBUS-IV satellite), and in six (configuration of the TOMS section of the SBUV/TOMS experiment on NIMBUS-G) narrow spectral regions in the ultraviolet part of the spectrum.

For this purpose, simulated measurements of the intensity of radiation back-scattered along the local nadir direction are generated with the computer algorithms making use of the method of direct numerical solution of the spherical harmonics approximation to the transfer equation. This is the scalar form of the transfer equation valid for a *pseudo-spherical* atmosphere with arbitrary vertical distribution of ozone, and with arbitrary height-distribution of up to two different kinds of aerosols. For this study and the study reported under the Technical Report: II of this contract, we worked with a total of 76 different models of the cloudfree earth-atmosphere system. For each of this atmospheric model, computations are performed for six different wavelengths, ten different positions of the sun, and several values of the Lambert reflectivity of the surface underlying the model.

Our investigations encompass changes in the following aerosol parameters:

(a) Imaginary part of the refractive index of the aerosol material; real part is assumed to have a value of 1.5;

(b) Stratospheric distribution, i.e., an aerosol vertical profile with all its particles confined to the parts of the atmosphere 12 km above the sea-level;

(c) Tropospheric distribution, i.e., an aerosol vertical profile with all its particles confined between the sea-level, and a level located 15 km above the sea-level;

(d) Size-distribution characteristics for the tropospheric aerosols, and;

(e) Models with stratospheric as well as tropospheric aerosol distributions with different size-distribution characteristics.

We find that the presence of stratospheric aerosols results in a significant underestimation of total ozone in an atmospheric colume when the solar zenith angle, at the time of measurements, is greater than 84°. The degree of this underestimation increases with an increase in aerosol content, in solar zenith angle, and in the actual ozone content of the column. On the other hand, the effect of tropospheric particulate pollutants on the total-ozone estimates is that of a small degree of overestimation, in most cases. Some recommendations whose implementation can assist in improving the accuracy of the satellite estimates of total ozone in the presence of significant aerosol contamination, are made in this report.

LIST OF FIGURES

No.	Title	Page
1	Variations of the normalized aerosol number-density [n(r) in number cm^{-3} μm^{-1}] as a function of the radius [r in μm] for the *Haze M*, *Haze L*, *Haze H*, and *Haze J* spherical polydispersions. The number-density is normalized to yield a unit value for the integral $\int_{r_{min}}^{r_{max}} n(r)\,dr$ for each case.	33
2	Variations of the volume scattering coefficient per average particle as a function of the wavelength (λ in μm) of the incident radiation for the *Haze M*, *Haze L*, *Haze H*, and *Haze J* spherical polydispersions. The refractive index (m) of the aerosol material is 1.5 - 0.0i.	36
3	Variations of the volume scattering coefficient (solid curve), and of the volume absorption coefficient (broken curve) per average particle as a function of the imaginary part (n_2) of the refractive index ($m = n_1 - i\,n_2$) of the aerosol material for the following spherical polydispersions: *Haze M*, *Haze L*, *Haze H*, and *Haze J*. $n_1 = 1.5$; $\lambda = 0.3398$ μm.	40

No.	Title	Page
4	Variations of the normalized phase function of a unit volume of the spherical polydispersions *Haze M*, *Haze L*, *Haze H*, and *Haze J*, as a function of the scattering angle. The upper (lower) set of curves is for the polydispersions made from material with a refractive index of 1.5 - 0.0i (1.5 - 0.1i).	44
5	Variations of the pressure thickness (mb km^{-1}, scale at the top), and of the stratospheric as well as tropospheric aerosol number-density (number km^{-1}) as a function of height for the atmospheric models used in our investigations. This diagram is for the models with 1×10^6, and 40×10^6 particles in the stratosphere, and troposphere, respectively. Curves for the models with aerosol contents different from those presented in this diagram, are obtained after shifting the appropriate curve to the left, or to the right, as necessary.	48
6	Variations, as a function of the wavelength (μm), of the changes in the intensity of radiation emerging along the nadir direction ($\theta = 0°$) due to the presence of stratospheric aerosols (Total amount: 20×10^6 particles; Size Distribution: *Haze H*) in the atmospheric model. Ω_{in} = 0.250 atm-cm; P_0 = 1,000 mb; R = 0.0. Solid curve: m = 1.5 - 0.0i; Dotted curve: m = 1.5 - 0.05i; Broken curve: m = 1.5 - 0.10i.	83

No.	Title	Page
7	Variations, as a function of the wavelength (μm), of the changes in the intensity of radiation emerging along the nadir direction ($\theta = 0°$) due to the presence of tropospheric aerosols (Total amount: 200×10^6 particles; Size distribution: *Haze L*) in the atmospheric model. $\Omega_{in} = 0.250$ atm-cm; $P_0 = 1{,}000$ mb; $R = 0.0$. Solid curve: $m = 1.5 - 0.0i$; Dotted curve: $m = 1.5 - 0.05i$; Broken curve: $m = 1.5 - 0.10i$.	94

LIST OF SYMBOLS

Symbol	Meaning
N_c	100 × logarithm of the ratio of computed intensities of the radiation at two wavelengths back-scattered along the nadir direction [see Eq. (4) of Dave, 1976 B].
NMX	Upper limit of the Legendre series representing the normalized, scattering phase function of a unit volume of spherical polydispersion; Eq. (3).
$P(\cos\Theta)$	Normalized, scattering phase function of a unit volume of spherical polydispersion; Eq. (3).
P_0	Pressure at the lower boundary (i.e., ground, or the cloud-top) of the atmospheric model.
$P_\ell(\cos\Theta)$	Legendre functions of the order ℓ.
R	Lambert reflectivity of the surface underlying the atmospheric model.
$\bar{R}$	*Effective surface albedo.*
$R^C_{\lambda,y}$	*Coarse effective surface albedo*, at the wavelength λ, determined by making use of the y mb surface-pressure tables.
$R^I_{\lambda,y}$	*Improved effective surface albedo*, at the wavelength λ, determined by making use of the y mb surface-pressure tables.

Symbol	Meaning
a	A parameter needed for specifying the size-distribution characteristics of a spherical polydispersion represented by a *modified gamma distribution;* Eq. (1).
b	Same as that of the symbol a above.
h	Height of an atmospheric level above the mean sea-level.
m	Refractive index of the aerosol material.
n_1	Real part of the refractive index (m).
n_2	Imaginary part of the refractive index (m).
n(r)	Number of aerosol particles per cc per one micrometer radius interval; Eqs. (1) and (2).
r	Radius of an aerosol particle assumed to be spherical in shape.
r_{max}	Upper limit for the size-distribution function of a spherical polydispersion.
r_{min}	Lower limit for the size-distribution function of a spherical polydispersion.
Δ	*Deviation* given by $1{,}000 \times [\Omega_e - \Omega_{in}]$.
Δ'	*Deviation* given by $1{,}000 \times [\Omega_e' - \Omega_{in}]$.
Θ	Scattering angle.

Symbol	Meaning
A_ℓ	Legendre coefficients of a series [see Eq. (3)] representing the normalized, scattering phase function of a unit volume of spherical polydispersion.
Ω_e	*Best ozone estimate.*
Ω_e'	*Improved, best ozone estimate.*
Ω_{in}	Total ozone amount in an atmospheric column of one sq cm cross-section when the lower boundary of the column is extended to 1,000 mb level whenever necessary; input ozone amount.
$\Omega^C_{x,y}$	*Coarse, total ozone amount* evaluated by making use of the simulated measurements at the x-th wavelength pair, and y mb surface-pressure tables.
$\Omega^I_{x,y}$	*Improved, total ozone amount* evaluated by making use of the simulated measurements at the x-th wavelength pair, and y mb surface-pressure tables.
α	Same as that of the symbol a above.
$\bar{\beta}^{(a)}$	Absorption cross-section of an average particle in a given spherical polydispersion (cm^2 per average particle).
$\bar{\beta}^{(sc)}$	Scattering cross-section of an average particle in a given spherical polydispersion (cm^2 per average particle).

Symbol	Meaning
γ	Same as that of the symbol a above.
θ	Angle which the direction of the emergent radiation makes with the local nadir direction.
θ_0	Solar zenith angle.
λ	Wavelength of the radiation.
ρ_{tp}	Change in the intensity of the radiation back-scattered along the nadir direction due to the presence of tropospheric aerosols in the model.
ρ_{st}	Change in the intensity of the radiation back-scattered along the nadir direction due to the presence of stratospheric aerosols in the model.
$\tau^{(s,R)}$	Normal, Rayleigh optical thickness due to scattering by molecules above the specified level of the atmospheric model.
$\tau^{(s,ST)}$	Normal, scattering optical thickness due to stratospheric aerosols above the specified level of the atmospheric model.
τ_b	Normal optical thickness of an atmospheric model due to scattering and absorption by molecules as well as aerosols.
$\tau_b^{(a)}$	Normal optical thickness of an atmospheric model due to absorption by the ozone molecules.

Symbol	Meaning
$\tau_b^{(a,ST)}$	Normal optical thickness of an atmospheric model due to absorption by the stratospheric aerosols.
$\tau_b^{(a,TP)}$	Normal optical thickness of an atmospheric model due to absorption by the tropospheric aerosols.
$\tau_b^{(s,R)}$	Normal Rayleigh optical thickness of an atmospheric model due to scattering by molecules.
$\tau_b^{(s,ST)}$	Normal optical thickness of an atmospheric model due to scattering by the stratospheric aerosols.
$\tau_b^{(s,TP)}$	Normal optical thickness of an atmospheric model due to scattering by the tropospheric aerosols.

LIST OF TABLES

No.	Title	Page
I.	Values of the constants appearing in Eq. (1) for three different *modified gamma distributions*.	31
II	Volume scattering cross-section $[\bar{\beta}^{(sc)}]$ of a unit volume of the spherical polydispersion.	37
III	Volume absorption cross-section $[\bar{\beta}^{(a)}]$ of a unit volume of the spherical polydispersion.	39
IV	Stratospheric and tropospheric aerosol contents of a column of one sq cm cross-section in 32 basic layers of the atmospheric models used in our investigations.	49
V	Scaling factors used for normalization of the total (scattering plus absorption) normal optical thickness due to the *Haze L*, and *Haze J* tropospheric aerosols at 0.3398 μm.	52
VI	Aerosol information (in a symbolic form, see Sec. 3.3) for various atmospheric models with P_0 = 1,000 mb, and Ω_{in} = 0.250 atm-cm.	56
VII	Aerosol information (in a symbolic form, see Sec. 3.3) for various atmospheric models with P_0 = 1,000 mb, and Ω_{in} = 0.450 atm-cm.	57

No.	Title	Page
VIII	Values of various normal optical thicknesses at 0.3125 μm for the atmospheric models with 1,000 mb surface pressure, and 0.250 atm-cm total ozone.	60
IX	Same as Table VIII but for 0.3175 μm wavelength.	61
X	Same as Table VIII but for 0.3312 μm wavelength.	62
XI	Same as Table VIII but for 0.3398 μm wavelength.	63
XII	Same as Table VIII but for 0.3600 μm wavelength.	64
XIII	Same as Table VIII but for 0.3800 μm wavelength.	65
XIV	Comparison of the *deviations* Δ and Δ' for a few selected atmospheric models with stratospheric aerosols. Ω_{in} = 0.250 atm-cm; P_0 = 1,000 mb; Procedure: SITC4.	71
XV	Same as Table XIV but for tropospheric aerosols.	73
XVI	Same as Table XV but for Procedure: SITD1.	74
XVII	Values of the *deviation* Δ' $[= 1{,}000 \times (\Omega_e' - \Omega_{in})]$ for the atmospheric models with Ω_{in} = 0.250 atm-cm, and stratospheric aerosols; P_0 = 1,000 mb. Procedure: SITC4; R = 0.1.	76
XVIII	Same as Table XVII but for R = 0.8.	77
XIX	Same as Table XVII but for Procedure: SITD1.	78

No.	Title	Page
XX	Same as Table XIX but for R = 0.8.	79
XXI	Same as Table XVIII but for Ω_{in} = 0.450 atm-cm.	85
XXII	Same as Table XX but for Ω_{in} = 0.450 atm-cm.	86
XXIII	Values of the *deviation* Δ' [= 1,000 × ($\Omega_e' - \Omega_{in}$)] for the atmospheric models with Ω_{in} = 0.250 atm-cm, and tropospheric aerosols; P_0 = 1,000 mb; R = 0.1.	90
XXIV	Same as Table XXIII but for R = 0.8.	91
XXV	Same as Table XXIII but for Ω_{in} = 0.450 atm-cm, and R = 0.8.	96
XXVI	Values of the *deviation* Δ' [= 1,000 × ($\Omega_e' - \Omega_{in}$)] for the atmospheric models with Ω_{in} = 0.250 atm-cm, and stratospheric as well as tropospheric aerosols; P_0 = 1,000 mb; R = 0.0.	98
XXVII	Same as Table XXVI but for Ω_{in} = 0.450 atm-cm.	99
XXVIII	Values of the *deviation* Δ' [= 1,000 × ($\Omega_e' - \Omega_{in}$)] for the atmospheric models with Ω_{in} = 0.250 atm-cm, and tropospheric aerosols of *Haze L*, and *Haze J* type size-distribution functions; P_0 = 1,000 mb; R = 0.0; Procedure: SITC4.	102

I. INTRODUCTION

1.1 *Background:* Ozone is perhaps the single most critical stratospheric constituent because its vertical distribution directly affects the deposition of energy in the stratosphere, while its total amount determines the ultraviolet radiation reaching the biosphere. Within the past decade, under the probability of increasing pollutant concentrations due to stratospheric commercial aviation and vertical transport of fluoro-chloro carbons, the stability of the stratospheric ozone layer has been questioned repeatedly in the scientific journals as well as in the press. Because of this, considerable attention is currently being given to the problem of reliable and continuous measurements of various characteristics of atmospheric ozone profiles on a global scale.

One of the techniques well suited for this purpose is a thorough analysis of the spectral signature of the earth-atmosphere system in the ultraviolet part (0.25 - 0.38 μm; 1 μm = 10^{-4} cm) of the electromagnetic spectrum. An accurate monitoring of this quantity on a global scale is being carried out for the last seven years, by Dr. D. F. Heath and his associates at NASA Goddard Space Flight Center with the help of the Backscatter Ultraviolet double monochromator (BUV) aboard the NIMBUS-IV satellite. A modified version of this BUV instrument is also aboard the Atmospheric Explorer satellite (AE-VI) which is currently in operation. A more sophisticated version of this BUV experiment referred to as SBUV/TOMS (Solar and Backscatter Ultraviolet/Total Ozone Mapping System), is scheduled to be aboard the NIMBUS-G satellite which in turn, is expected to be operational within a year from now.

Estimation of total ozone in an atmospheric column from the multi-wavelength measurements of the ultraviolet radiation backscattered by it, is not a trivial problem for several reasons. First, a relatively noise-free set of spectrally pure measurements in several predetermined pseudo-monochromatic regions is required with an accurate knowledge of the instrument's position and attitude in space and time. Second, there are a good number of atmospheric unknowns which can modulate the signal in an undeterminable manner. Besides the total ozone to be estimated, some of the other unknowns are its vertical profile, reflectivity of the underlying surface and its directional as well as wavelength dependence, pressure at the base of atmospheric column (i.e., surface pressure or the effective cloud-top pressure), aerosols, water droplets, ice crystals, trace gases with significant absorption in the spectral regions of immediate interest, and nonhomogeneity in the field of view due to one or more of these factors.

Some aspects of this complex problem were first investigated by Dave and Mateer (1967) with simulated measurements restricted to the Rayleigh-scattering models of the earth-atmosphere system. Based on this prior study, Mateer, Heath, and Krueger (1971) developed a procedure for estimating total ozone, in an atmospheric column underneath the NIMBUS-IV satellite, from measurements of the back-scattered ultraviolet radiation in five pseudomonochromatic spectral regions (viz., 0.3125, 0.3175, 0.3312, 0.3398, and 0.3800 μm). They then used their procedure for estimating total ozone for a sample of 320 cases of approximate coincidences

(in space as well as in time) of the NIMBUS-IV data, and *ground-truth* measurements of total ozone with the Dobson Spectrophotometer. They found the satellite values to be lower than the corresponding Dobson values by about 0.025 atm-cm, on the average. Some cases were also reported where the difference between an individual satellite and Dobson total-ozone approximate-coincidence measurement was as high as 0.060 atm-cm. They argued that a part of this difference is due to a lack of perfect coincidence between the *ground-truth*, and the satellite data. Based on their experience with the analysis of the NIMBUS-IV data, they recommended an additional measurement at 0.3600 μm for the TOMS section of the SBUV/TOMS.

Henceforth, the total-ozone estimation procedure for the analysis of the actual BUV data mentioned in the preceding paragraph, will be referred to as the NASA total-ozone estimation procedure. This procedure is for interpreting five spectral measurements of the earth-atmosphere system along the local nadir direction, in terms of the *effective surface albedo* ($\bar{R}$), and the *best ozone estimate* (Ω_e), i.e., the best estimate of the total ozone content of the atmospheric column for which measurements are available. The foundation of this NASA total-ozone estimation procedure is two sets of tables computed after taking into account all orders of scattering, and using a modified version of the procedure discussed by Dave (1964). The first (second) set of tables is for aerosol-free models with different ozone content Ω_{in}, but for 1.0 (0.4) atmosphere surface pressure. [In the remaining part of this report, we will

refer to these 1.0 (0.4) atmosphere surface pressure tables as 1,000 (400) mb tables.] It is thus evident that the contributions to the outgoing radiation due to the extinction by aerosols are only approximately accounted for through the concept of the *effective surface albedo* which may or may not be equal to the actual reflectivity of the surface underneath the column.

Investigations undertaken by us under the NASA/GSFC Contract No. NAS5-23556 cover the following aspects of the problem of estimating total ozone from the spectral measurements of the ultraviolet reflectivity of the earth-atmosphere system:

(1) A critical analysis of the current, NASA, total-ozone estimation procedure along with recommendations for increasing the reliability and confidence level of the ozone data;

(2) Proposing of a total-ozone estimation procedure for the interpretation of six-wavelength TOMS measurements in terms of $\bar{R}$ and Ω_e, and a preliminary testing there of (this aspect will be restricted to TOMS measurements along the direction of local nadir, only); and

(3) Estimation of the effect of atmospheric aerosols on the values of total ozone obtained with the help of procedures mentioned in (1) and (2), above.

The aforementioned aspects are studied by making use of the simulated measurements of the earth-atmospheric systems of known physical properties.

1.2 *Algorithm for the Computations of Intensity:* From the background of the subject investigation presented in the preceding section, it is clear that the first requirement is of an algorithm capable of providing intensity of the radiation back-scattered by realistic models of the earth-atmosphere system, along the local nadir direction. These values of intensity are required for about one-hundred atmospheric models. For each of these models, data are required for 10 different directions of the incident solar radiation, and for six different wavelengths. Hence, the algorithm must be fairly efficient. It should also be capable of providing numerical values of about three significant-figure accuracy.

Such an algorithm was developed, debugged, and tested under this contract. It is fully documented in the Technical Report: I of this contract (Dave, 1977 A). This algorithm makes use of the method of the direct numerical solution of the Spherical Harmonics Approximation to the scalar form of the equation of radiative transfer (Dave and Canosa, 1974; Dave, 1974; as well as Dave and Armstrong, 1974). Its purpose is to evaluate the azimuth-independent component of intensity of the scattered radiation emerging at the top of a nonhomogeneous *pseudo-spherical* model of the terrestrial atmosphere. This azimuth-independent component of intensity is evaluated for 18 different nadir angles (θ) of the directions of observation of the TOMS instrument aboard a satellite with a nominal altitude of 955 km. It should be pointed out that this azimuth-independent component of intensity is equal to the intensity of the emergent radiation whenever $\theta = 0°$ (i.e., observation along the local

nadir direction), and/or whenever the sun is at local zenith (i.e., solar zenith angle, $\theta_0 = 0°$). As mentioned earlier, we are only interested in the values of the intensity along the local nadir for our present investigation. Values in the remaining 17 directions are computed to assist in the future studies.

Our basic atmospheric model is that of a plane-parallel atmosphere of homogeneous character and infinite extent along the horizontal directions. It is of finite optical extent along the vertical direction to which any nonhomogeneity due to scattering and/or absorption is confined. By *pseudo-spherical*, we mean that the sphericity of the atmosphere is only partly accounted for; viz., by computing attenuation suffered by the incoming solar radiation arriving at an atmospheric level for the actual spherical case. This modification then permits computations for the case of the sun at the local horizon ($\theta_0 = 90°$). Refraction of the incoming ray is not taken into account.

Our algorithm is primarily for an atmospheric model consisting of 32 nonhomogeneous layers. The height (h) of the base of these layers above the mean sea-level is given as follows: h = 0 (1) 25 km, 25 (5) 50 km, and 50 (10) 60 km. The top of the atmosphere is assumed to be located at a height of 70 km above the mean sea-level. This 32-layer model will have the maximum surface pressure at the lower boundary. [For our work, this 32-layer model has a surface pressure (P_0) of 1,000 mb.] Models with P_0 less than 1,000 mb are generated by deleting one, or more, bottom-most layers of the 32-layer model. Provision is made

for assigning ozone amount (in atm-cm), and the aerosol number-contents of a one sq cm cross-section column to each of these layers. Two different types of aerosol (assumed to exist in the form of a spherical polydispersion) height-distributions can be accommodated by this algorithm. A type of the aerosol is specified by its size distribution function, and the refractive index of its material.

These atmospheric models are assumed to rest on a surface obeying Lambert's law of reflection. According to this law, the radiation reflected by the surface is unpolarized and is isotropically distributed, independent of the direction and the state of the radiation incident upon it. The Lambert reflectivity (R) of such a surface is defined as the ratio of the flux of energy reflected by it, to that of the incident energy upon it. The following quantities are computed by the algorithm as the further use of this data in the total-ozone estimation investigations require values of the intensity of the emergent radiation for any arbitrary value of the parameter, R:

Azimuth-independent component of the intensity emerging at the top of the atmospheric model resting on a perfectly absorbing surface ($R \approx 0$);

Direct plus diffuse transmission by the atmospheric model in the direction θ when the model is illuminated from below by the isotropic radiation; and,

A quantity representing the diffuse flux reflectivity of the model for the case of its isotropic illumination from below.

All these quantities are dependent upon the wavelength (λ) of the radiation under scrutiny, and also upon various parameters of the atmospheric model under investigation. Furthermore, the first two of these quantities also depend upon the parameters θ, and θ_0. The expression for computing values of the intensity for an atmospheric model resting on a Lambert surface with reflectivity R, from the values of the three quantities listed above, can be found on p. 15 of Dave (1976 A).

The first two quantities listed in the preceding paragraph are computed for ten different values of the parameter θ_0, viz., 0°, 45°, 60°, 70°, 75.6°, 79.6°, 82.5°, 84.7°, 86.7°, and 90°. A given set of computations consists of all these quantities at six different wavelengths, viz., 0.3125, 0.3175, 0.3312, 0.3398, 0.3600, and 0.3800 μm. This entire set of data for a given model is assigned a unique number, and is stored on a disk for future use.

Various programs for this algorithm were written in FORTRAN IV language, and were compiled under the FORTRAN H extended, Optimizer Level 2, compiler. The execution of the programs was carried out via an IBM 2741 Communication Terminal (or an IBM 3270 Visual Display Station) attached to an IBM 370/145 computer running under VM-CMS. A 3-megabyte virtual machine with an attached 3330 disk space of 40 cylinders was used for this purpose.

1.3 *Analysis of the Total-Ozone Estimation Procedure:* In Sec. 1.1, we mentioned that a computer program (NASA total-ozone estimation procedure) is being currently used at NASA Goddard Space Flight Center (NASA/GSFC)

for the estimation of total ozone from the measurements of the ultraviolet radiation backscattered by a terrestrial atmospheric column. This NASA program was modified by us primarily to take advantage of several special features of the simulated measurements generated by the algorithm described in Sec. 1.2. Some of these special features of such simulated measurements are as follows: availability of measurements at solar zenith angles for which basic tables are stored, and simultaneous measurements at all wavelengths. In fact, several versions of this NASA total-ozone estimation procedure were produced with minor changes to study the effect of various aspects of the total-ozone estimation problem (Dave, 1976 B).

One of these modified versions of the NASA total-ozone estimation procedure, referred to as the SITC4 procedure (Dave, 1976 B), is recommended by us for forming the basis for the proposed reanalysis of the entire BUV data, and is also used by us here for studying the effect of atmospheric aerosols on total-ozone estimations (see Sec. IV of this report). This SITC4 procedure is for estimating values of the *effective surface albedo* ($\bar{R}$), and the *best ozone estimate* (Ω_e) from the simulated BUV measurements in five well-defined spectral regions (centered at 0.3125, 0.3175, 0.3312, 0.3398, and 0.3800 μm) when these simulated measurements are for the atmospheric models resting on surfaces with spectrally-independent, Lambert reflectivity.

Out of the five spectral regions for which measurements are made in the BUV configuration, the first four regions are located within the ozone absorption band. Thus, only the measurement at 0.3800 μm is ini-

tially available for extracting information about the surface reflectivity. The effect of various unknowns listed in the third paragraph of Sec. 1.1 is minimized by taking the ratio of measured intensities in two near-by wavelength regions, one of which exhibits stronger absorption by ozone than the other. For the BUV configuration, the wavelength pairs 0.3312 - 0.3125 μm (Pair 1), and 0.3398 - 0.3175 μm (Pair 2) are therefore used for extracting information on the total ozone content of the atmospheric column. Observations at the first wavelength pair are generally used for the total-ozone estimation when these observations are not for very large values of the parameter θ_0. For values of θ_0 greater than about 80°, contribution to the shorter wavelength (0.3125 μm) of the first wavelength pair starts coming from the parts of the atmosphere located within, and above, the ozone layer. Consequently, the first wavelength pair starts losing its sensitivity to changes in total ozone amount at large θ_0. Under such circumstances, observations at the second wavelength pair are used for the total ozone estimation.

Even when relatively noise-free measurements unaffected by aerosols and other unspecified atmospheric constitutents are available, the problem of estimating total ozone in the atmospheric column under the NIMBUS-IV satellite requires knowledge of the surface pressure (P_0), and reflectivity of the surface at five wavelengths listed above. The BUV observations contain very little information about the parameter P_0, if any. It is therefore considered appropriate to use two sets of tables (one set for 1,000 mb surface pressure models, and the other for 400 mb sur-

face pressure models). As mentioned in Sec. 1.1, these sets are for Rayleigh-scattering models of the terrestrial atmosphere.

The first pass with the set of five observations through the SITC4 procedure then provides values of the *coarse effective surface albedo* $\left[R^{C}_{0.3800,y}\right]$, and the *coarse total ozone amount* $\left[\Omega^{C}_{x,y}\right]$. The subscript y stands for the set of the surface pressure tables (1,000 mb or 400 mb) used in the evaluation of the quantity. The other subscript (x) represents the wavelength pair. Computations of the quantity $\Omega^{C}_{x,y}$ does require values of the quantity $R^{C}_{\lambda,y}$ at λ = 0.3125, 0.3175, 0.3312, and 0.3398 μm. Since only the value of $R^{C}_{\lambda,y}$ at 0.3800 is available, it is necessary to assume that the quantity $R^{C}_{\lambda,y}$ is independent of λ.

Depending upon the sensitivity of the wavelength pairs to changes in the ozone amount in the regions of immediate interest, one of the $\Omega^{C}_{x,y}$ values is used to compute the *improved effective surface albedo* at 0.3398 μm $\left[R^{I}_{0.3398,y}\right]$ using measurement at 0.3398 μm. We then make a second pass through the SITC4 procedure to obtain values of the *improved total ozone amounts*, $\Omega^{I}_{x,y}$ after assuming that the quantity $R^{I}_{\lambda,y}$ is independent of λ.

In the absence of any information about the magnitude of the parameter P_0, the value of the *effective surface albedo* $\left[\bar{R} = 0.5\left(R^{I}_{\lambda,1000} + R^{I}_{\lambda,400}\right)\right]$ is used to obtain the value of the *best ozone estimate* (Ω_e) from those of $\Omega^{I}_{x,1000}$ and $\Omega^{I}_{x,400}$ for the selected wavelength pair. Further information about this SITC4 procedure can be found in Sec. 5.1 of the Technical Report: II of this contract (Dave, 1976 B).

The total ozone estimation procedure used by us for analyzing the simulated measurements of the SBUV/TOMS configuration (5 BUV wavelengths plus an additional measurement at 0.3600 μm) is named the SITD1 procedure, and is also fully described in the aforementioned Technical Report. The main difference between the SITD1 and SITC4 procedure is in assigning values to the quantities $R^C_{\lambda,y}$ and $R^I_{\lambda,y}$ at the shorter wavelengths. For the SITC4 procedure, it was necessary to assume that the quantities $R^C_{\lambda,y}$ and $R^I_{\lambda,y}$ are independent of λ. For the SITD1 procedure, since we have an additional measurement in the spectral region with a very insignificant amount of absorption by ozone, we compute values of $R^C_{\lambda,y}$ at λ = 0.3125, 0.3175, 0.3312, and 0.3398 μm by linearly extrapolating the straight line of the $R^C_{\lambda,y}$ vs. λ in 0.3600 - 0.3800 μm region. Values of $R^I_{\lambda,y}$ at λ = 0.3125, 0.3175, and 0.3312 μm are obtained after a quadratic extrapolation of the $R^I_{\lambda,y}$ vs. λ curve in 0.3398 - 0.3800 μm region.

Simulated measurements for the aerosol-free atmospheric models with different ozone amounts (Ω_{in} in atm-cm) and surface pressures (a total of 34 models) were used to compute values of R and Ω_e for 10 different values of θ_0 listed earlier, and 8 different values (R = 0.0, 0.1, 0.2, 0.3, 0.4, 0.6, 0.8, and 1.0) of the Lambert reflectivity of the underlying surface. This R parameter was taken to be independent of wavelength. The SITC4 and SITD1 procedures were used for this purpose. Comparison of Ω_e so computed with the corresponding value of Ω_{in} showed that the absence of any information about the parameter P_0 gen-

erally results in a significant overestimation ($\Omega_e > \Omega_{in}$) of total ozone under two conditions. One of these conditions corresponds to the occurrence of high surface pressure with high surface reflectivity, and the other to that of the occurrence of low surface pressure with low surface reflectivity. It was also shown that this difference between Ω_e and Ω_{in} can be very insignificant if the value of P_0 is available (and is used in the determination of Ω_e) at the place and time of observation. Henceforth, we will refer to the total ozone amount determined after making use of the P_0 information as *improved, best ozone estimate* (Ω_e'). If $P_0 = 1{,}000$ mb, $\Omega_e' = \Omega^I_{x,1000}$ when a proper value of the subscript x is selected after studying the sensitivity of both wavelength pairs to change in the ozone amount.

Values of Ω_e obtained with the SITC4 and SITD1 procedures were found to be mutually comparable (on the average) as long as simulated measurements were generated for models with their underlying surfaces having λ-independent reflectivity. For the simulated measurements for models with their underlying surfaces having spectrally-dependent reflectivity, values of Ω_e obtained with the SITD1 procedure were found to compare much more favorably with the corresponding values of Ω_{in}, than those obtained with the SITC4 procedure.

1.4 *General Outline of this Report:* The main purpose of this Final Report for the NASA/GSFC Contract No. NAS5-23556, is to study the effect of atmospheric aerosols on the estimation of total ozone content of an atmospheric column, from the simulated measurements of the intensity of

the ultraviolet radiation backscattered by it at five (BUV configuration), and at six (SBUV/TOMS) different wavelengths along the nadir direction. The total ozone content of an atmospheric column corrected for the expected ozone content between its lower boundary and the 1,000 mb level, is represented by the symbol Ω_{in} (Dave, 1976 B; p. 7). A value of the total ozone determined from the analysis of the simulated measurements is referred to as the *best ozone estimate* (Ω_e) when the information about the pressure at the base of the atmospheric column, and at the place and time of measurements, is not used in the analysis. If such information about the surface pressure is used in the analysis, the value of total ozone then determined is called the *improved, best ozone estimate*, and is represented by the symbol Ω_e'. The total-ozone estimationtion procedure used for the analysis of the simulated BUV (SBUV/TOMS)-configuration measurements, is referred to as the SITC4 (SITD1) procedure.

The physical characteristics of aerosols used in our investigations are described in Sec. 2 of this report. This section also deals with the optical properties of these aerosol models in the spectral region of interest, viz., 0.3100 - 0.3800 μm.

In Sec. 3, we provide information about the height-distribution characteristics of two types of aerosols (viz., stratospheric and tropospheric) used in our models of the terrestrial atmosphere. Information about the total aerosol content and spectral dependence of the scattering, as well as absorption, normal optical thicknesses of various atmospheric models, is also provided in this section. A complete description

of an atmospheric model includes information about the pressure (P_0) at its lower boundary, Lambert reflectivity (R) of the underlying surface, total ozone content (Ω_{in}), solar zenith angle (θ_0), and the information about refractive indices, size-distribution functions, height-distribution characteristics, and the total aerosol contents of the stratospheric as well as tropospheric aerosols. Results presented in this final report are for the models with 1,000 mb surface pressure; therefore, it is unnecessary to refer to this parameter. Results are presented for two values of the parameter Ω_{in}, viz., 0.250 and 0.450 atm-cm. However, the results for models with Ω_{in} = 0.450 atm-cm are presented for a few limited cases only. It is therefore considered appropriate to mention this parameter only when some confusion is likely to develop in understanding of the discussion. A concise nomenclature for representing various parameters of the aerosols in a model is given in Sec. 3.3. Values of the parameters R and θ_0 will be given as an adjective describing a specific case for a given model.

Effect of aerosols on the values of total ozone estimated using the SITC4 and SITD1 procedures is discussed in Sec. 4 by presenting results of the *deviation* Δ, and the *deviation* Δ' which are defined by $1{,}000 \times (\Omega_e - \Omega_{in})$, and $1{,}000 \times (\Omega_e' - \Omega_{in})$, respectively. Since the effect of aerosols on the ozone estimate is found to be of somewhat smaller magnitude to that of the parameter P_0, our discussion of the results is generally for the quantity Δ'. Selected results from computations for 40 different atmospheric models with different types of aero-

sols, and with 10 different values of θ_0 (viz., 0°, 45°, 60°, 70°, 75.6°, 79.6°, 82.5°, 84.7°, 86.7°, and 90°), as well as 8 different values of R (viz., 0.0, 0.1, 0.2, 0.3, 0.4, 0.6, 0.8, and 1.0), are presented in Sec. 4.

II. AEROSOL MODELS

2.1 *Physical Characteristics:* Aerosols of a unit volume of air are assumed to exist in the form of a spherical polydispersion of known size-distribution characteristics, and made of a material of known refractive index ($m = n_1 - i\,n_2$) with respect to air.

The assumption about the sphericity of aerosol particles is primarily made because of the ready availability of extensive datasets for them. The exact theory (Mie, 1908) used for this purpose permits calculations of all characteristics of the scattered radiation field of a sphere illuminated by a parallel beam of radiation. There is some evidence in the published literature suggesting that the scattering by randomly-oriented irregular particles can not be approximated with that due to spheres of the same refractive index. However, this sphericity assumption can not be expected to modify our conclusion in any significant manner.

The real part (n_1) of the refractive index of the aerosol materials encountered in the terrestrial atmosphere is known to vary from 1.3 to 2.0. However, the effect of this parameter on our total-ozone estima-

tions can be expected to be of secondary importance only. We have therefor considered it appropriate to restrict our present investigations to a value of 1.5 for this parameter n_1. The imaginary part can also vary in the range 0.0 - 0.5. However, at large values of n_2, the atmospheric aerosols tend to become opaque to the incident radiation. Hence, the absorption cross-section of a unit volume of a given spherical polydispersion increases rapidly with n_2 in the lower range of the parameter n_2, but very little in its upper range. Based on these considerations, we have used the following five values of the parameter n_2: viz., 0.0, 0.01, 0.03, 0.05, and 0.10. These values of n_2 are expected to cover a wide range of conditions encountered in the terrestrial atmosphere. It should be added that, for a given set of simulated observations for estimating total ozone (i.e., for a given θ_0, R case of a given atmospheric model), we have assumed that the refractive index of the aerosol material is independent of wavelength.

For specifying the size-distribution characteristics of spherical polydispersions of aerosol, we have considered four different size-distribution functions commonly used in simulation studies. The first three of these size-distribution functions are represented by a *modified gamma distribution* (Deirmendjian, 1969) for which the normalized, aerosol number-density [n(r) in number per cc per one micrometer radius interval] is given by the following equation:

$$n(r) = a\, r^{\alpha} \exp(-b\, r^{\gamma}) , \qquad (1)$$

where r is the radius of the spherical particle in micrometers. Values of the constants a, α, b and γ for the size-distribution functions called *Haze H*, *Haze L*, and *Haze M*, are given in Table I. The lower (r_{min}), and the upper (r_{max}) cut-offs for these functions are 0.001, and 7.0 μm, respectively.

TABLE I. Values of the constants appearing in Eq. (1) for three different *modified gamma distributions*.

Size-distribution function	Constants appearing in Eq. (1)			
	a	α	b	γ
Haze H	4.00000×10^3	2.0	20.0000	1.0
Haze L	4.97570×10^4	2.0	15.1186	0.5
Haze M	5.33333×10^2	1.0	8.9443	0.5

The fourth size-distribution function is a discontinuous function called the *Junge* size-distribution function (Bullrich, 1964). It will be referred to as *Haze J* in this report. Values of n(r) for this function are given by the following equation:

$$\left.\begin{aligned} n(r) &= 8.33 \qquad \text{for } 0.02 \le r \le 0.1, \\ \text{and} \\ n(r) &= 8.33(0.1/r)^4 \qquad \text{for } 0.1 \le r \le 7.0 \end{aligned}\right\}. \tag{2}$$

Further information about the rationale behind the use of these size-distribution functions for representing n(r) vs. r characteristics of the terrestrial aerosols, can be found in the publication by Bullrich (1964), and by Deirmendjian (1969). It will suffice to state here that the *Haze H* function is expected to describe, adequately, the size-distribution characteristics of the aerosol particles found in the lower stratosphere. The *Haze M* function is expected to represent the size-distribution characteristics of aerosols found in the lower levels of large coastal areas. The size-distribution characteristics of aerosols in the lower troposphere over large continental areas are represented by the *Haze L*, and *Haze J* functions.

Variations of n(r) vs. r for the four different kinds of size-distribution functions described in the preceding paragraphs, are shown in Fig. 1 on a log-log scale. With the values of various constants given above, the integral

$$\int_{r_{min}}^{r_{max}} n(r)\, dr$$

has a value of unity for the *Haze H*, *Haze L*, and *Haze M* functions, and a value of 0.944 for the *Haze J* function.

2.2 *Cross-Sections:* The optical properties of the scalar (without polarization aspects) field of the radiation scattered by a unit volume of a given spherical polydispersion, are fully represented by two sets of quantities. The first set of quantities contains the scattering cross-

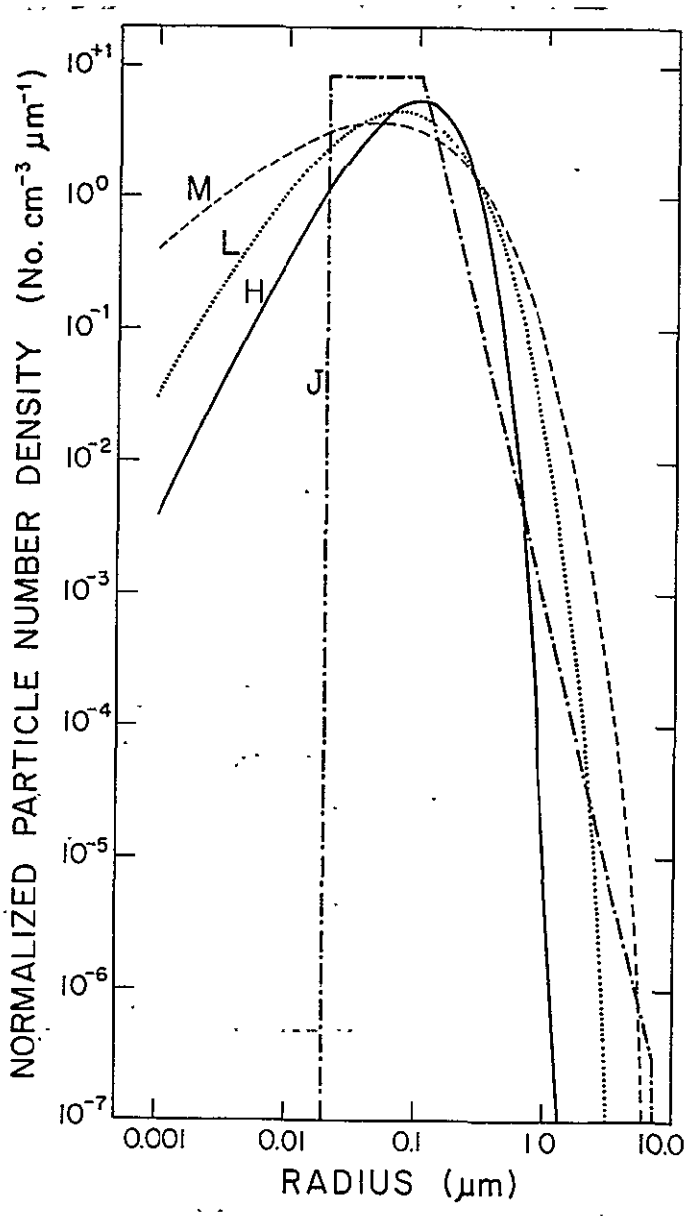

Fig. 1. Variations of the normalized aerosol number-density [n(r) in number cm^{-3} μm^{-1}] as a function of the radius (r in μm) for the *Haze M*, *Haze L*, *Haze H*, and *Haze J* spherical polydispersions. The number-density is normalized to yield a unit value for the integral $\int_{r_{min}}^{r_{max}} n(r)\,dr$ for each case.

section $[\bar{\beta}^{(sc)}]$, and the absorption cross-section $[\bar{\beta}^{(a)}]$ of an average particle in the spherical polydispersion (cm^2 per average particle). (These cross-sections are also referred to as coefficients in the literature.) The second set of quantities consists of a series of normalized Legendre coefficients $[\Lambda_\ell]$ describing the directional characteristics of the radiation scattered by the polydispersion according to the following equation:

$$P(\cos\Theta) = \sum_{\ell=0}^{NMX} \Lambda_\ell P_\ell(\cos\Theta) \; . \qquad (3)$$

The quantity $P(\cos\Theta)$ on the left hand side of this equation is called the normalized phase function (see p. 19 of Dave, 1976 A). The functions $P_\ell(\cos\Theta)$ are the well-known Legendre functions whose argument is the cosine of the angle (Θ) between the directions of the incidence, and scattering.

The quantities $\bar{\beta}^{(sc)}$, $\bar{\beta}^{(a)}$, Λ_ℓ, and NMX are functions of various parameters necessary to describe a given spherical polydispersion, and also of the refractive index ($m = n_1 - i\,n_2$) of the polydispersion material.

All these quantities were computed from the basic data representing the scattering and absorption characteristics of spheres of known size parameter (circumference/wavelength of the incident radiation), and made from materials of known refractive indices. Such basic data were available for a large number of values of the size parameter [0.02 (0.02) 10.00, 10.0 (0.1) 130.0, and 130.0 (0.5) 150.0] and for each of five values of the

refractive indices listed in the third paragraph of Sec. 2.1, from previous investigations in the atmospheric radiation field carried out at the Palo Alto Scientific Center.

Further information about the normalized, scattering phase function $[P(\cos\Theta)]$ for various types of aerosols will be given in Sec. 2.3.

In Fig. 2, we have shown variations of the quantity $\bar{\beta}^{(sc)}$, as a function of the wavelength (λ), for four spherical polydispersions described in Sec. 2.1. The results presented in this diagram are those of the aerosol particles made from a substance with a refractive index of 1.5 - 0.0i. The scattering cross-section per average particle of the spherical polydispersion called *Haze M* and *Haze L*, increases with an increase of wavelength in the spectral region of concern to our present investigation, i.e., 0.31 - 0.38 μm. On the other hand, $\bar{\beta}^{(sc)}$ vs. λ curve for the *Haze H* spherical polydispersion exhibits a broad maximum around 0.35 μm wavelength, and that for the *Haze J* shows a decrease in the values of $\bar{\beta}^{(sc)}$ with an increase in λ.

Values of $\bar{\beta}^{(sc)}$ for all six wavelengths of interest, and for four different spherical polydispersions are given in Table II for three values of the parameter m, viz., 1.5 - 0.00i, 1.5 - 0.05i, and 1.5 - 0.10i. It can be seen that the general trends of $\bar{\beta}^{(sc)}$ vs. λ curves for m = 1.5 - 0.00i shown in Fig. 2 for the size distribution functions *Haze M*, *Haze L*, and *Haze J*, are also present in the corresponding curves for m = 1.5 - 0.05i, and 1.5 - 0.10i. Increase in the imaginary part of the refractive index of the *Haze H* polydispersion material results in a

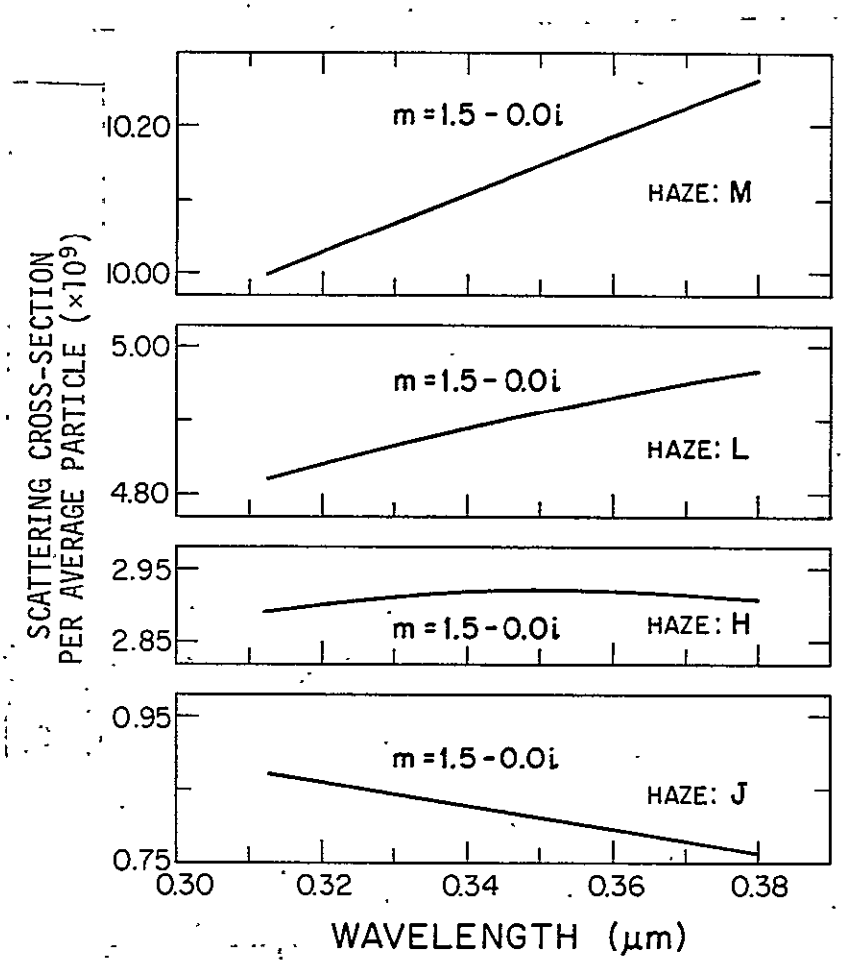

Fig. 2. Variations of the scattering cross-section per average particle as a function of the wavelength (λ in μm) of the incident radiation for the *Haze M*, *Haze L*, *Haze H*, and *Haze J* spherical polydispersions. The refractive index (m) of the aerosol material is equal to 1.5 - 0.0i.

TABLE II. Scattering cross-section $[\overline{\beta}^{(sc)}]$ per average particle of the spherical polydispersion.

Refractive index	Wavelength in μm	10^9 × volume scattering cross-section for			
		Haze H	*Haze L*	*Haze M*	*Haze J*
1.5 - 0.00i	0.3125	2.8907	4.8218	9.997	0.8724
	0.3175	2.8972	4.8345	10.017	0.8638
	0.3312	2.9106	4.8678	10.073	0.8404
	0.3398	2.9157	4.8876	10.107	0.8259
	0.3600	2.9179	4.9305	10.186	0.7926
	0.3800	2.9069	4.9681	10.262	0.7611
1.5 - 0.05i	0.3125	2.0148	3.0128	5.7211	0.6277
	0.3175	2.0249	3.0298	5.7466	0.6224
	0.3312	2.0490	3.0751	5.8089	0.6076
	0.3398	2.0614	3.1025	5.8492	0.5984
	0.3600	2.0822	3.1639	5.9430	0.5769
	0.3800	2.0919	3.2202	6.0348	0.5562
1.5 - 0.10i	0.3125	1.6247	2.5649	5.1845	0.5263
	0.3175	1.6318	2.5753	5.1970	0.5221
	0.3312	1.6487	2.6032	5.2316	0.5106
	0.3398	1.6575	2.6202	5.2533	0.5034
	0.3600	1.6725	2.6584	5.3049	0.4864
	0.3800	1.6799	2.6936	5.3558	0.4699

shift of the maximum in the $\bar{\beta}^{(sc)}$ vs. λ curve towards longer wavelengths. Thus, values of $\bar{\beta}^{(sc)}$ for the *Haze H* polydispersion with $m = 1.5 - 0.05i$ and $1.5 - 0.10i$ show an increase with increase of λ.

In Table III, we have given values of the volume absorption cross-scection $[\bar{\beta}^{(a)}]$ of an average particle in the spherical polydispersion *Haze H, Haze L, Haze M,* and *Haze J* for six wavelengths of interest to the total-ozone estimation problem. These values are given for three representative values of the parameter m, viz., $1.5 - 0.00i$, $1.5 - 0.05i$, and $1.5 - 0.10i$. For $n_2 = 0$, $\bar{\beta}^{(a)} \equiv 0$ for all size-distribution functions, and for all wavelengths as there is no absorption by the aerosol particle in this particular case. For $n_2 > 0$, values of $\bar{\beta}^{(a)}$ generally decrease with an increase of the wavelength λ. The only exception to this statement is the case with $m = 1.5 - 0.10i$ of the *Haze M* spherical polydispersion which shows an increase in $\bar{\beta}^{(a)}$ with an increase of wavelength.

In Fig. 3, we have plotted values of $\bar{\beta}^{(sc)}$ and $\bar{\beta}^{(a)}$ as a function of the imaginary part of the refractive index of the spherical polydispersion material. The solid (broken) curves are for the volume scattering (absorption) cross-section per an average particle in the polydispersion. Results presented in this figure are for an incident radiation of 0.3398 μm wavelength. Values of $\bar{\beta}^{(sc)}$ show a decrease with an increase of the parameter n_2, while those of $\bar{\beta}^{(a)}$ show opposite trends. However, the rate of increase or decrease is very small in the upper range of the parameter n_2. In fact, $\bar{\beta}^{(a)}$ is always smaller than the

TABLE III. Absorption cross-section $[\bar{\beta}^{(a)}]$ per average particle of the spherical polydispersion.

Refractive index	Wavelength in μm	10^9 × volume absorption cross-section for			
		Haze H	*Haze L*	*Haze M*	*Haze J*
1.5 - 0.00i	0.3125	0.	0.	0.	0.
	0.3175	0.	0.	0.	0.
	0.3312	0.	0.	0.	0.
	0.3398	0.	0.	0.	0.
	0.3600	0.	0.	0.	0.
	0.3800	0.	0.	0.	0.
1.5 - 0.05i	0.3125	0.7347	1.7114	4.1786	0.2278
	0.3175	0.7281	1.7045	4.1733	0.2257
	0.3312	0.7108	1.6855	4.1579	0.2201
	0.3398	0.6992	1.6734	4.1478	0.2167
	0.3600	0.6741	1.6449	4.1226	0.2091
	0.3800	0.6502	1.6165	4.0960	0.2020
1.5 - 0.10i	0.3125	1.0110	2.0691	4.6246	0.3176
	0.3175	1.0057	2.0667	4.6279	0.3153
	0.3312	0.9910	2.0596	4.6361	0.3091
	0.3398	0.9817	2.0546	4.6405	0.3054
	0.3600	0.9595	2.0417	4.6487	0.2967
	0.3800	0.9375	2.0274	4.6539	0.2885

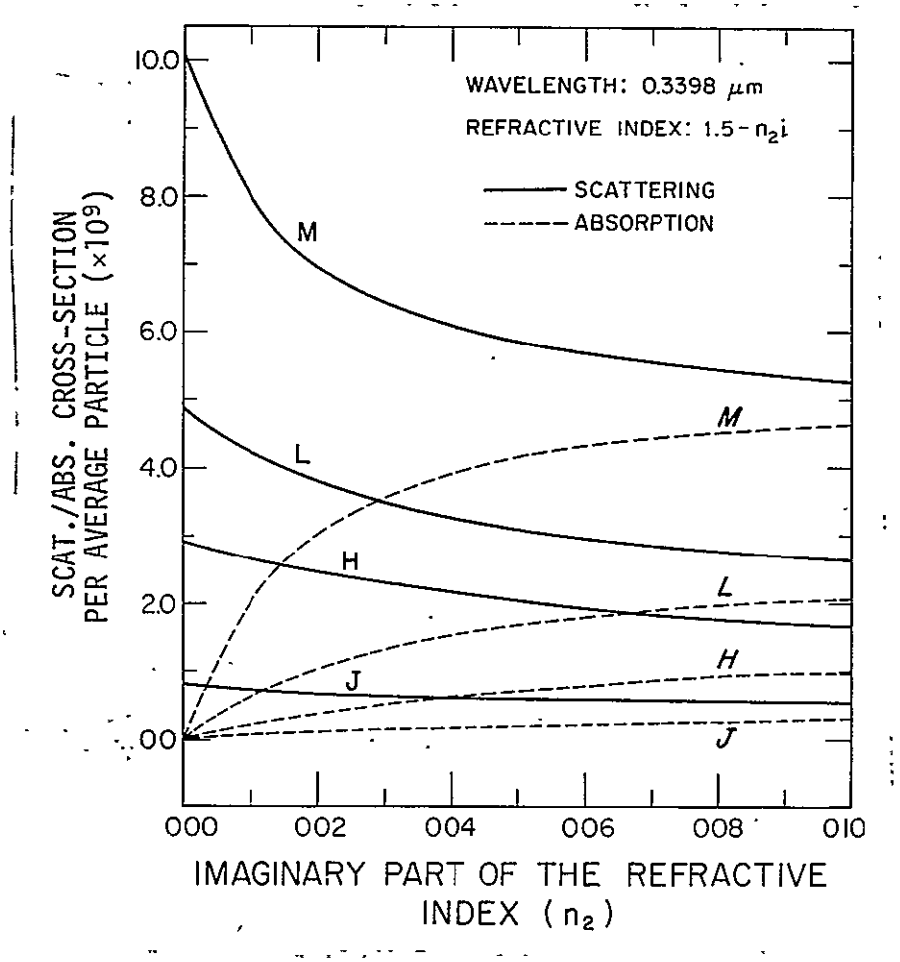

Fig. 3. Variations of the scattering coefficient (solid curve), and of the absorption coefficient (broken curve) per average particle as a function of the imaginary part (n_2) of the refractive index ($m = n_1 - i\,n_2$) of the aerosol material for the following spherical polydispersions: *Haze M*, *Haze L*, *Haze H*, and *Haze J*. $n_1 = 1.5$; $\lambda = 0.3398$ μm.

corresponding value of $\bar{\beta}^{(sc)}$ for a given n_2, size-distribution function and λ combination.

Before closing this section, it should be pointed out that the changes in $\bar{\beta}^{(sc)}$ and $\bar{\beta}^{(a)}$ discussed in the preceding paragraphs for the spectral region $0.31 - 0.38$ μm, are rather small in magnitude. The maximum change encountered is of the order of 15% over a 0.07 μm change in λ.

2.3 *Normalized Phase Function:* In the preceding section, we mentioned that the directional distribution of the intensity of the radiation scattered by a unit volume of spherical polydispersion, is represented by the normalized scattering phase function $P(\cos\Theta)$; see Eq. (3). The quantity Θ represents the angle between the directions of the incident and scattered radiations. This phase function is expanded in a Legendre series whose coefficients (Λ_ℓ) depend upon the size distribution characteristics, and refractive index of the polydispersion. The upper limit of this series (viz., the quantity NMX) required for an *adequate* representation of the phase function, also depends upon this parameter but, is primarily determined by the size parameter of the largest sphere responsible for contributing significantly to values of $P(\cos\Theta)$ in various directions.

Typical plots of Λ_ℓ vs. ℓ for various spherical polydispersions and wavelength combinations (Canosa and Penafiel, 1973) show that Λ_ℓ increases with ℓ, initially. However, a further increase in the sub-

script ℓ results in a rapid decrease of Λ_ℓ. The actual slope of the log Λ_ℓ vs. ℓ curve at high values of ℓ is determined by the size distribution parameters of the spherical polydispersion, and the wavelength of illumination. From this discussion, we see that values of Λ_ℓ at very high values of the subscript ℓ are not necessary for an *adequate* representation of the phase function within any reasonable accuracy.

Use of the computer program described in another NASA/GSFC Contract Report (Dave, 1972) results in the generation Λ_ℓ terms whose absolute values are of the order of 10^{-20}, or even smaller, at large values of the subscript ℓ. For the spherical polydispersions *Haze H*, the upper limits of the Legendre series of phase functions for various λ and $m(= n_1 - i\,n_2)$ combinations, and as generated by this program (Dave, 1972), were found to fall in the range 65 - 75. For the *Haze L* polydispersion, this range was found to be 160 - 190. For the remaining two polydispersions whose radiation fields receive significant contributions from spheres as large as 6 μm in radii (i.e., *Haze M* and *Haze J*), this range was found to be 270 - 325. A very significant reduction in these upper limits, without any significant effect on $P(\cos\Theta)$ values, could be obtained by terminating the series for a given case (specified by λ, m, and the size-distribution parameters) at a value of the subscript ℓ such that absolute values of all Λ_ℓ's above this value of ℓ, are less than 10^{-5}. With this criterion, the range for the upper limits of the Legendre series for *Haze H* polydispersions could be reduced from 65 - 75, to 40 - 45.

It was found that an *adequate* representation of the phase function for a given case can be maintained with an accuracy of at least first three significant figures, after still lowering of the upper limit, NMX. For this purpose, we compared values of $P(\cos\Theta)$ obtained after terminating the series, for a given case, at NMX-80, NMX-70, $\cdots$, NMX-10, and NMX. A total of 181 values of Θ given by $\Theta = 0°\ (1°)\ 180°$ was used for this purpose. With this 2-step examination of Λ_ℓ output for the case specified by *Haze L*, 1.5 - 0.01i, and 0.3125 μm, we succeeded in lowering the upper limit of the Legendre series of its phase function from 190 to 149 (10^{-5} criterion), to 119 (3 SF reproduction of the phase function criterion), without any undesirable effects on $P(\cos\Theta)$. Similar reductions in the upper limit of the Legendre series for phase functions of other cases were also obtained after carrying out above-mentioned procedures. We feel that this analysis of Λ_ℓ vs. ℓ output for various cases is necessary for obtaining a very significant reduction in the computational load with an assurance that no deterioration, in the quality of ultimate results, has occurred.

In Fig. 4, we have plotted values of $P(\cos\Theta)$, as a function of the scattering angle Θ, for the spherical polydispersions *Haze H*, *Haze L*, *Haze M*, and *Haze J* illuminated by 0.3398 μm radiation. The upper (lower) set of the curves is for polydispersions made from a material with a refractive index of 1.5 - 0.0i (1.5 - 0.1i). Results are presented only for the angular range of immediate interest, viz., 90° - 180°. For the observations along the local nadir, the direction of interest varies from

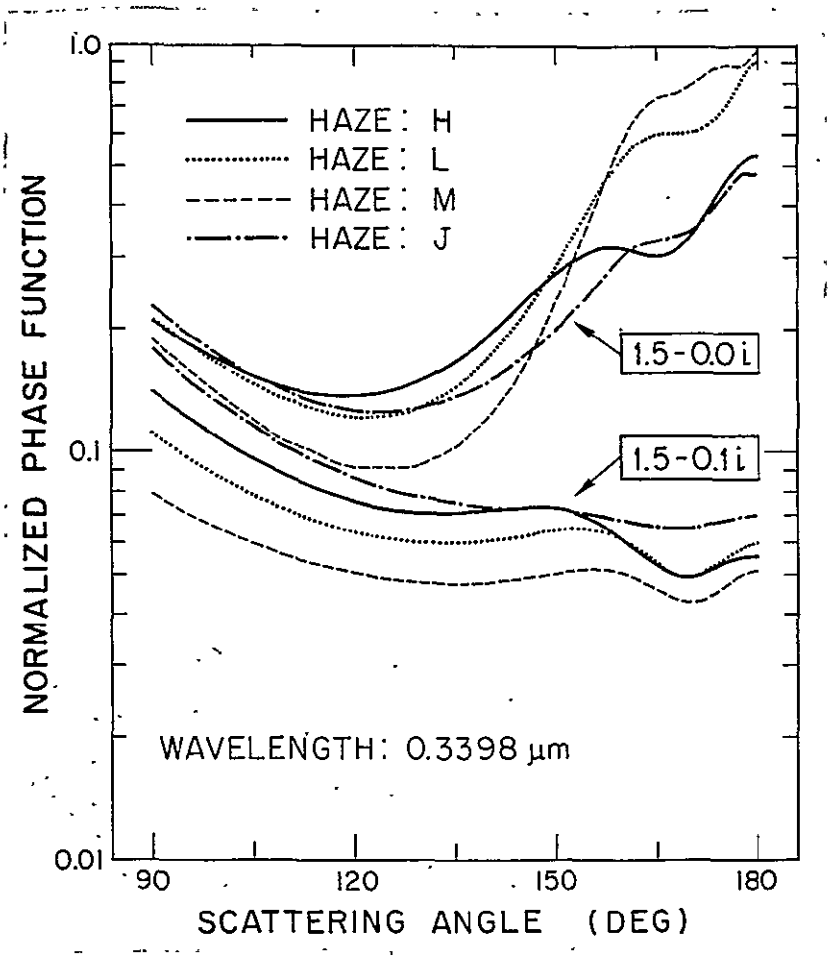

Fig. 4. Variations of the normalized phase function of a unit volume of the spherical polydispersions *Haze M*, *Haze L*, *Haze H*, and *Haze J*, as a function of the scattering angle. The upper (lower) set of curves is for the polydispersions made from material with a refractive index of 1.5 - 0.0i (1.5 - 0.1i). An integration of the scattering phase function over a solid angle of 4π, yields a value of 4π.

$\Theta = 180°$ to $\Theta = 90°$, as the solar zenith angle (θ_0) is changed from 0° to 90°.

For $m = 1.5 - 0.0i$, slopes of the $P(\cos\Theta)$ vs. Θ curves in the angular region 150° - 180° are greater for the *Haze L* and *Haze M* polydispersions, than those for the other two. An increase in the imaginary part of the refractive index results in the disappearance of the relatively broad peak, in the backward direction, for all four cases.

Before concluding this section, we would like to comment on the upper limit (r_{max}) for the size-distribution function *Haze J*. According to Fig. 1 and also Eq. (2), $r_{max} = 7.0$ μm for this polydispersion. As it can be seen from Fig. 1, for values of $r > 6$ μm, the slope of $n(r)$ vs. r curve for the *Haze J* polydispersion is the smallest of all. In fact, this slope is such that particles with $r > 7.0$ μm may contribute, to some extent, to computed values of $P(\cos\Theta)$, $\bar{\beta}^{(sc)}$, and $\bar{\beta}^{(a)}$ for this dispersion at all wavelengths, and for all refractive indices. Particles of radius greater than 7.0 μm can be sustained under average atmospheric conditions. Thus, the upper limit of the size-distribution function *Haze J* is definitely arbitrary. (With respect to this, it should be pointed out that the polydispersions *Haze L* and *Haze M* tend to provide lower bounds for the giant aerosol number-density encountered under average, tropospheric conditions.) In order to investigate the effect of r_{max} on computed values of $P(\cos\Theta)$ and $\bar{\beta}^{(sc)}$ for the spherical polydispersion *Haze J*, a new set of calculations were carried out for all six wavelengths but for $m = 1.5 - 0.00i$ only. We found

that an increase in the value of r_{max} for the *Haze J* polydispersion from 7.0 μm to 10.0 μm results in an increase of $\bar{\beta}^{(sc)}$ by about 0.3%, but those of $P(\cos\Theta)$ in the forward direction ($\Theta = 0°$) by as much as 24%. In other directions, values of $P(\cos\Theta)$ of the *Haze J* polydispersion obtained with the aforementioned values of r_{max} were found to agree, on the average, within ±1%.

III. ATMOSPHERIC MODELS

3.1 *Height-Distribution Characteristics of Aerosols:* On pp. 21 - 24 of the Technical Report: II of this contract (Dave, 1976 B), we provided information about the geometric thickness, pressure thickness, and ozone contents of 32 different basic layers of various aerosol-free models used in our investigations. The latter information is provided for ten different atmospheric models whose total ozone content (Ω_{in}) is varied from 0.200 to 0.650 atm-cm, in steps of 0.050 atm-cm. Our investigations on the effect of aerosols on the values of total ozone estimated from the backscattered radiation measurements, are restricted to models with Ω_{in} = 0.250, and 0.450 atm-cm. Furthermore, surface pressure (P_0) at the lower boundary of these atmospheric models is taken to be 1,000 mb. These two aerosol-free models, viz., P_0 = 1,000 mb and Ω_{in} = 0.250 atm-cm, and P_0 = 1,000 mb and Ω_{in} = 0.450 atm-cm, are assigned the numbers 3 and 7, respectively, during our previous investigations.

For studying the effect of aerosols on total-ozone estimations, we have used two aerosol-content vs. height curves which are expected to represent vertical profiles of aerosols encountered in the terrestrial atmosphere under average conditions. One of these aerosol-content vs. height curves is void of any aerosol particles in the lower atmosphere, and is therefore referred to as the stratospheric distribution. The other one with its aerosol content confined to the lower parts of the atmosphere only, is referred to as the tropospheric distribution.

In Fig. 5, we have shown the variations of the pressure thickness (mb km^{-1}), and the aerosol number-density (number cm^{-2} km^{-1}) for the stratospheric as well as tropospheric distributions as a function of height (km). Numerical values of the stratospheric as well as tropospheric aerosol contents of a column of one sq cm cross-section in each of the 32 basic layers of the atmospheric models, are given in Table IV. Results presented in Fig. 5 and Table IV are for the models with 1×10^6 aerosol particles in the stratosphere, and 40×10^6 particles in the troposphere. Similar data for the models with total aerosol contents different from those presented here, are obtained after multiplying the aerosol-content vector of a given distribution by the appropriate scalar factor. Thus, for our present investigations, a change in the total aerosol content of the atmospheric column for a given type of aerosol implies *no* change in the vertical profile of that aerosol distribution.

The vertical profile of the stratospheric distribution used for our investigations shows a broad maximum between 18 and 25 km, and a rapid

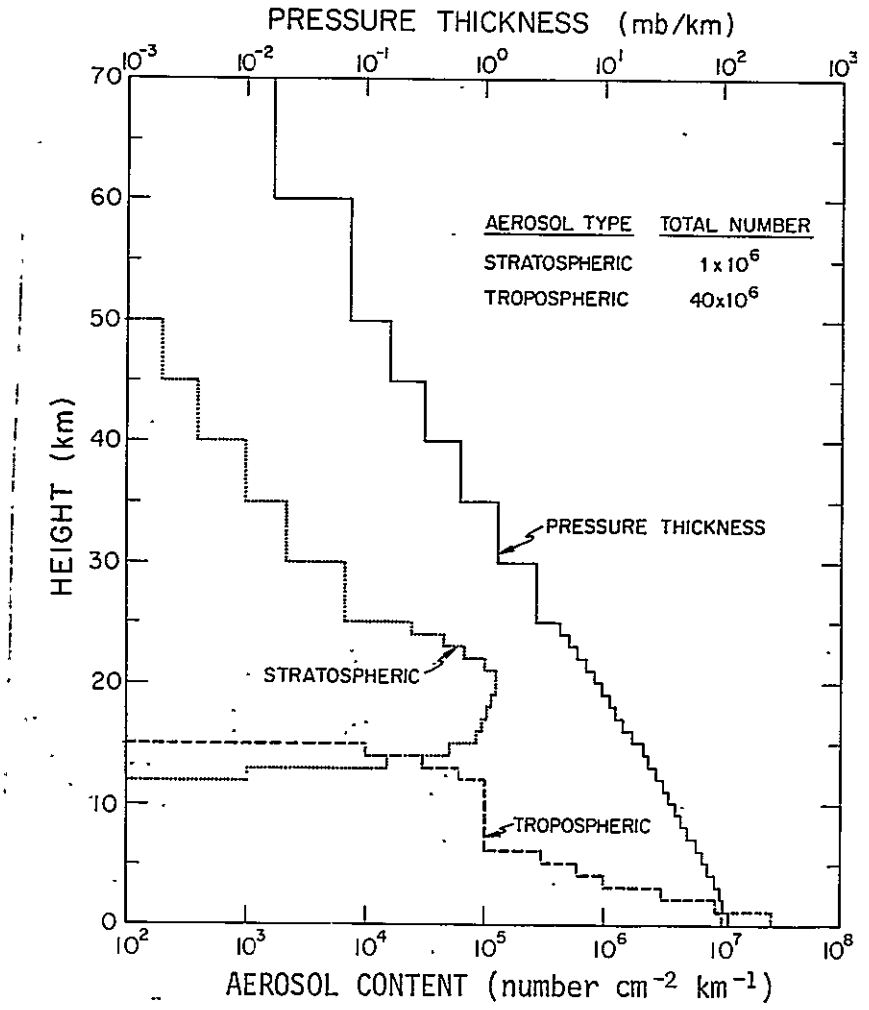

Fig. 5. Variations of the pressure thickness (mb km^{-1}, scale at the top), and of the stratospheric as well as tropospheric aerosol number-density (number cm^{-2} km^{-1}) as a function of height for the atmospheric models used in our investigations. This diagram is for the models with 1×10^{6}, and 40×10^{6} particles in one sq. cm. column of the stratosphere and troposphere, respectively. Curves for the models with aerosol contents different from those presented in this diagram, are obtained after shifting the appropriate curve to the left or the right as necessary.

TABLE IV. Stratospheric and tropospheric aerosol contents of a column of one sq cm cross-section in 32 basic layers of the atmospheric models used in our investigations..

These data are for the models with 1×10^6 aerosol particles in the stratosphere and 40×10^6 particles in the troposphere. Similar data for the models with total aerosol contents different from those presented in this table, are obtained by multiplying content of all layers for a given distribution by an appropriate factor.

Layer number	Aerosol content		Layer number	Aerosol content	
	Stratos.	Tropos.		Stratos.	Tropos.
1	0.	0.	17	8.50×10^4	0.
2	0.	0.	18	5.00	1.00×10^4
3	1.00×10^3	0.	19	1.50	3.00
4	2.00	0.	20	1.00×10^3	6.00
5	5.00	0.	21	0.	1.00×10^5
6	1.10×10^4	0.	22	0.	1.00
7	3.40	0.	23	0.	1.00
8	2.40	0.	24	0.	1.00
9	4.50	0.	25	0.	1.00
10	6.80	0.	26	0.	1.00
11	1.00×10^5	0.	27	0.	3.00
12	1.24	0.	28	0.	6.00
13	1.24	0.	29	0.	1.00×10^6
14	1.14	0.	30	0.	3.00
15	1.03	0.	31	0.	8.90
16	9.40×10^4	0.	32	0.	2.55×10^7

decrease in the aerosol number-density with increase of height above 25 km level. The aerosol number-density for the tropospheric distribution shows a very rapid decrease with an increase of height in the 0 - 5 km region, but very little change in the 6 - 12 km region.

3.2 *Total Aerosol Contents of Various Models:* In the preceding section, we mentioned that a change in the total aerosol content of an atmospheric column for a given type of aerosols (stratospheric or tropospheric) does not involve any change in its vertical profile. This limitation is imposed primarily for understanding the effect of changing a given aerosol parameter on the values of total ozone estimated from the simulated measurements of the ultraviolet radiation backscattered by the earth-atmosphere system.

Our investigations related to changes in the stratospheric aerosol parameters is restricted to only one size-distribution function, viz., *Haze H*. Several values of the imaginary part of the refractive index of the polydispersion material are used, but these changes do not call for any adjustment of the total stratospheric aerosol content of the atmospheric column. We have used three different values for the total stratospheric aerosol content parameter, viz., 1×10^6, 5×10^6, and 20×10^6. As mentioned earlier, stratospheric aerosol contents of columns in basic layers for the 5×10^6 (20×10^6) case are obtained after multiplying values in the second and fifth columns of Table IV by a scalar factor of 5.0 (20.0).

For our investigations related to changes in the tropospheric aerosol parameters, we have considered it proper to use two different size-distribution functions (viz., *Haze L* and *Haze J*) after analysis of the results presented in Figs. 2 and 4. For our total tropospheric aerosol content, we have used two different values (viz., 40×10^6 and 200×10^6) in conjunction with the size-distribution function *Haze L*.

From the results presented in Fig. 2, Tables II and III, it can be seen that the volume scattering and volume absorption cross-sections of an average particle for the *Haze L* polydispersion for a given λ,m combination are significantly different from those for the *Haze J* polydispersion. Furthermore, the rate of change of $\bar{\beta}^{(sc)}$ [or $\bar{\beta}^{(a)}$] with λ is also dependent upon values of the parameter m, and the size-distribution function. These differences between values of $\bar{\beta}^{(sc)}$ and $\bar{\beta}^{(a)}$ for the *Haze L* and *Haze J* polydispersions, and their dependence on λ and m, create problems during interpretation of the total-ozone estimation results. If we wish to study the effect of changes in the size-distribution function on the estimated values of total ozone and in so doing we hold the total tropospheric aerosol content constant, we have changed not only the size-distribution function of the tropospheric aerosols, but also the total normal optical thicknesses of models at all wavelengths. A change in the size-distribution function of the tropospheric aerosols from *Haze L* to *Haze J* results in a reduction of the total, tropospheric-aerosol, normal optical thickness by a factor of about 6.

In order to minimize the effect of changes in optical thickness introduced as a result of changes in the size-distribution function, values of the total (scattering plus absorption) normal optical thickness due to tropospheric aerosols were made equal at $\lambda = 0.3398$ μm for the set of models whose results are to be intercompared. Values of the scaling factors used for such normalization are given in Table V. As for example, the results for the model with the spherical polydispersion *Haze L* having $m = 1.5 - 0.05i$ and 200×10^6 (scaling factor: 5.0) particles, become comparable with those of the model with the spherical polydispersion *Haze J* having the same value of the parameter m, but 1172×10^6 (scaling factor: 29.2950) particles. This normalization yields a value of 0.95518 for the total (scattering plus absorption) normal optical thickness due to the

TABLE V. Scaling factors used for normalization of the total (scattering plus absorption) normal optical thickness due to the *Haze L* and *Haze J* tropospheric aerosols at 0.3398 μm.

Refractive index	*Haze L*		*Haze J*	
	Scaling factor	Total aerosol content	Scaling factor	Total aerosol content
1.5 - 0.00i	1.0	40×10^6	5.9181	237×10^6
1.5 - 0.00i	5.0	200×10^6	29.5905	1184×10^6
1.5 - 0.05i	1.0	40×10^6	5.8590	234×10^6
1.5 - 0.05i	5.0	200×10^6	29.2950	1172×10^6
1.5 - 0.10i	1.0	40×10^6	5.7805	231×10^6
1.5 - 0.10i	5.0	200×10^6	28.9025	1156×10^6

Haze L and *Haze J* aerosols of $m = 1.5 - 0.05i$, at 0.3398 μm only. At other wavelengths, this normal optical thickness for these two types of aerosols have different values.

3.3 *Nomenclature:* From the discussion in Secs. 3.1 and 3.2, it is evident that a complete and unambiguous description of the modeled conditions at the time of a given set of simulated measurements, requires specification of a large number of parameters. In order to discuss the results in a precise manner, it is therefore necessary to identify modeled conditions with one, or more, symbols.

The first parameter is related to the pressure at the lower boundary of the atmospheric model under investigation. This parameter referred to as the surface pressure, or the cloud-top pressure, is designated by the symbol P_0. Fortunately, all results presented in this report are restricted to models with $P_0 = 1{,}000$ mb. It is therefore unnecessary to refer to this parameter during our discussion.

The second parameter is the total ozone content (Ω_{in}) of a unit atmospheric column of the model when its lower boundary is extended down to 1,000 mb level, whenever necessary. We have used two different values for this parameter, viz., 0.250 and 0.450 atm-cm. We intend to present results for these two values of Ω_{in} in separate paragraphs. Therefore, this parameter will be explicitly identified only where a confusion is likely to develop.

Next, we have a series of parameters identifying various properties of aerosols which are assumed to exist in the form of spherical polydispersions with known size-distribution characteristics. Four different size-distribution functions (viz., *Haze H*, *Haze L*, *Haze M*, and *Haze J*, see Sec. 2.1) are mentioned in this report. We have assigned a fixed value of 1.5 to the real part (n_1) of the refractive index ($m = n_1 - i\,n_2$) of the aerosol material. Two different vertical profiles (viz., stratospheric and tropospheric, see Sec. 3.1) representing variations of the aerosol concentration with height are used in our investigations. A change in the total aerosol content of one of these two types of aerosols involves only a relative displacement of the corresponding vertical profile curve along a direction perpendicular to the height axis. Thus, we require a mentioning of only three parameters for each type of aerosol. These three parameters are as follows: total aerosol content of one sq cm cross-section column of the atmospheric model for a given type of aerosol, its size-distribution function, and the imaginary part (n_2) of the refractive index of the aerosol material.

For the identification of all variable characteristics of aerosols in an atmospheric model, we have generated a two-part symbol. These two parts of the symbol are connected by the character "-". The first (second) part of the symbol represents the aforementioned three properties of the stratospheric (tropospheric) aerosols. Each part of the symbol has the form nnn X mm if the kind represented by that part is present in that model. (The quantity nnn X mm for a given kind of aerosol is set

to zero for a model free of that particular kind.) The numerals nnn (sometimes n, nn, or nnnn) represent the total aerosol content of the given type of aerosols in the model. The letter X specifies the last part of the name of the size-distribution function, i.e., X = *H*, *L*, *M*, or *J*. The numerals mm are equal to 100 n_2.

Aerosol information about various atmospheric models used in our investigations is given in Table VI and VII for Ω_{in} = 0.250 and 0.450 atm-cm, respectively. These tables also serve the purpose of an easy identification of various computer outputs which are referred to by model numbers.

Two additional parameters remain to be identified for an unambiguous description of all conditions at the time of a given set of simulated measurements. One of these parameters is the solar zenith angle θ_0. The other parameter is the spectrally-independent, Lambert reflectivity (R) of the surface underlying the atmospheric model under investigation.

Thus, when we say "the $\theta_0 = 60°$, R = 0.4 case for the 20 H 05 - 200 L 10 model," we imply as follows: This set of simulated measurements is for an atmospheric model illuminated at its top by a beam of the direct solar radiation making an angle of 60° with the local zenith, while the model rests on a surface with the spectrally-independent, Lambert reflectivity of 0.4. Furthermore, a one sq cm cross-section of this atmospheric column contains 20 million particles whose concentration vs. height features are represented by the stratospheric profile of

TABLE VI. Aerosol information (in a symbolic form, see Sec. 3.3) for various atmospheric models with P_0 = 1,000 mb and Ω_{in} = 0.250 atm-cm.

Model number	Aerosol information
3	0 – 0
25	1 H 00 – 0
26	5 H 00 – 0
45	20 H 00 – 0
27	1 H 05 – 0
28	5 H 05 – 0
46	20 H 05 – 0
47	1 H 10 – 0
48	5 H 10 – 0
49	20 H 10 – 0
23	0 – 40 L 00
24	0 – 200 L 00
29	0 – 40 L 05
30	0 – 200 L 05
54	0 – 40 L 10
55	0 – 200 L 10
50	0 – 237 J 00
51	0 – 1184 J 00
52	0 – 234 J 05
53	0 – 1172 J 05
56	0 – 231 J 10
57	0 – 1156 J 10
58	20 H 05 – 200 L 05
59	20 H 10 – 200 L 10

TABLE VII. Aerosol information (in a symbolic form, see Sec. 3.3) for various atmospheric models with P_0 = 1,000 mb and Ω_{in} = 0.450 atm-cm.

Model number	Aerosol information
7	0 - 0
60	1 H 00 - 0
61	5 H 00 - 0
62	20 H 00 - 0
63	1 H 05 - 0
64	5 H 05 - 0
65	20 H 05 - 0
66	1 H 10 - 0
67	5 H 10 - 0
68	20 H 10 - 0
69	0 - 40 L 00
70	0 - 200 L 00
71	0 - 40 L 05
72	0 - 200 L 05
73	0 - 40 L 10
74	0 - 200 L 10
75	20 H 05 - 200 L 05
76	20 H 10 - 200 L 10

Fig. 5, and 200 million particles whose concentration vs. height features are represented by the tropospheric profile of the same figure. The size-distribution characteristics of the stratospheric (tropospheric) aerosols are those of a spherical polydispersion called *Haze H (Haze L)*. Besides, these stratospheric and tropospheric polydispersions are made from materials with a refractive index of 1.5 - 0.05i and 1.5 - 0.10i, respectively. No information about the parameter Ω_{in} (total ozone) is provided here as its magnitude is obvious at that point in the discussion.

3.4 *Optical Thicknesses for the Models with 0.250 atm-cm Total Ozone:* The total normal optical thickness (τ_b) of an atmospheric model is the sum of the following six normal optical thicknesses:

$\tau_b^{(s,R)}$: Normal Rayleigh optical thickness due to scattering by molecules;

$\tau_b^{(a)}$: Normal optical thickness due to absorption by the ozone molecules (for its height-distribution characteristics, see Tables I and II of Dave, 1976 B);

$\tau_b^{(s,ST)}$: Normal optical thickness due to scattering by the stratospheric aerosols;

$\tau_b^{(a,ST)}$: Normal optical thickness due to absorption by the stratospheric aerosols;

$\tau_b^{(s,TP)}$: Normal optical thickness due to scattering by the tropospheric aerosols; and

$\tau_b^{(a,TP)}$: Normal optical thickness due to absorption by the tropospheric aerosols.

All these optical thicknesses are functions of the composition of the atmospheric model and the wavelength of the radiation under investigation.

Values of these optical thicknesses for all atmospheric models with 0.250 atm-cm total ozone as used in our study are given in Tables VIII, IX, X, XI, XII, and XIII for λ = 0.3125, 0.3175, 0.3312, 0.3398, 0.3600, and 0.3800 μm, respectively.

3.5 *Optical Thicknesses for the Models with 0.450 atm-cm Total Ozone:* The only reason for computing the emergent radiation fields for dusty (with aerosols) models with different ozone amounts, is to study the relative effect of a given aerosol condition under different ozone situations. We therefore selected several atmospheric models with 1,000 mb surface pressure and 0.250 atm-cm total ozone, and increased their ozone content to 0.450 atm-cm. On comparing the aerosol information given in Tables VI and VII, we find that models with the *Haze J* aerosols are not included in this specific aspect of our investigation.

A use of the aforementioned procedure for the generation of a 0.450 atm-cm total-ozone model from a given 0.250 atm-cm total-ozone model, results in no change in values of the normal optical thicknesses $\tau_b^{(s,R)}$, $\tau_b^{(s,ST)}$, $\tau_b^{(a,ST)}$, $\tau_b^{(s,TP)}$, and $\tau_b^{(a,TP)}$. Furthermore, all optical thicknesses at λ = 0.3800 μm also remain unchanged as there is no absorption

TABLE VIII. Values of various normal optical thicknesses at 0.3125 μm for the atmospheric models with 1,000 mb surface pressure and 0.250 atm-cm total ozone.

$\tau_b^{(s,R)} = 1.02000$ $\tau_b^{(a)} = 0.41750$

Aerosols	$\tau_b^{(s,ST)}$	$\tau_b^{(a,ST)}$	$\tau_b^{(s,TP)}$	$\tau_b^{(a,TP)}$	τ_b
1 H 00 - 0	0.00289	0.	0.	0.	1.44039
5 H 00 - 0	0.01445	0.	0.	0.	1.45195
20 H 00 - 0	0.05781	0.	0.	0.	1.49531
1 H 05 - 0	0.00201	0.00073	0.	0.	1.44025
5 H 05 - 0	0.01007	0.00367	0.	0.	1.45124
20 H 05 - 0	0.04030	0.01469	0.	0.	1.49249
1 H 10 - 0	0.00162	0.00101	0.	0.	1.44013
5 H 10 - 0	0.00812	0.00506	0.	0.	1.45068
20 H 10 - 0	0.03249	0.02022	0.	0.	1.49021
0 - 40 L 00	0.	0.	0.19287	0.	1.63037
0 - 200 L 00	0.	0.	0.96435	0.	2.40185
0 - 40 L 05	0.	0.	0.12051	0.06846	1.62647
0 - 200 L 05	0.	0.	0.60257	0.34229	2.38235
0 - 40 L 10	0.	0.	0.10259	0.08276	1.62286
0 - 200 L 10	0.	0.	0.51297	0.41382	2.36429
0 - 237 J 00	0.	0.	0.20653	0.	1.64403
0 - 1184 J 00	0.	0.	1.03264	0.	2.47014
0 - 234 J 05	0.	0.	0.14711	0.05339	1.63799
0 - 1172 J 05	0.	0.	0.73554	0.26694	2.43998
0 - 231 J 10	0.	0.	0.12169	0.07342	1.63261
0 - 1156 J 10	0.	0.	0.60845	0.36712	2.41307
20 H 05 - 200 L 05	0.04030	0.01469	0.60257	0.34229	2.43734
20 H 10 - 200 L 10	0.03249	0.02022	0.51297	0.41382	2.41700

TABLE IX. Values of various normal optical thicknesses at 0.3175 μm for the atmospheric models with 1,000 mb surface pressure and 0.250 atm-cm total ozone.

$\tau_b^{(s,R)} = 0.95700$ $\tau_b^{(a)} = 0.22750$

Aerosols	$\tau_b^{(s,ST)}$	$\tau_b^{(a,ST)}$	$\tau_b^{(s,TP)}$	$\tau_b^{(a,TP)}$	τ_b
1 H 00 - 0	0.00290	0.	0.	0.	1.18740
5 H 00 - 0	0.01449	0.	0.	0.	1.19898
20 H 00 - 0	0.05794	0.	0.	0.	1.24244
1 H 05 - 0	0.00202	0.00073	0.	0.	1.18725
5 H 05 - 0	0.01012	0.00364	0.	0.	1.19826
20 H 05 - 0	0.04050	0.01456	0.	0.	1.23956
1 H 10 - 0	0.00163	0.00101	0.	0.	1.18714
5 H 10 - 0	0.00816	0.00503	0.	0.	1.19769
20 H 10 - 0	0.03264	0.02011	0.	0.	1.23725
0 - 40 L 00	0.	0.	0.19338	0.	1.37788
0 - 200 L 00	0.	0.	0.96690	0.	2.15139
0 - 40 L 05	0.	0.	0.12119	0.06818	1.37387
0 - 200 L 05	0.	0.	0.60596	0.34091	2.13137
0 - 40 L 10	0.	0.	0.10301	0.08267	1.37018
0 - 200 L 10	0.	0.	0.51506	0.41334	2.11290
0 - 237 J 00	0.	0.	0.20449	0.	1.38899
0 - 1184 J 00	0.	0.	1.02245	0.	2.20695
0 - 234 J 05	0.	0.	0.14585	0.05290	1.38325
0 - 1172 J 05	0.	0.	0.72927	0.26449	2.17825
0 - 231 J 10	0.	0.	0.12073	0.07290	1.37812
0 - 1156 J 10	0.	0.	0.60363	0.36449	2.15262
20 H 05 - 200 L 05	0.04050	0.01456	0.60596	0.34091	2.18643
20 H 10 - 200 L 10	0.03264	0.02011	0.51506	0.41334	2.16565

TABLE X. Values of various normal optical thicknesses at 0.3312 μm for the atmospheric models with 1,000 mb surface pressure and 0.250 atm-cm total ozone.

$\tau_b^{(s,R)} = 0.80000$ $\tau_b^{(a)} = 0.04375$

Aerosols	$\tau_b^{(s,ST)}$	$\tau_b^{(a,ST)}$	$\tau_b^{(s,TP)}$	$\tau_b^{(a,TP)}$	τ_b
1 H 00 – 0	0.00291	0.	0.	0.	0.84666
5 H 00 – 0	0.01455	0.	0.	0.	0.85830
20 H 00 – 0	0.05821	0.	0.	0.	0.90196
1 H 05 – 0	0.00205	0.00071	0.	0.	0.84651
5 H 05 – 0	0.01025	0.00355	0.	0.	0.85755
20 H 05 – 0	0.04098	0.01420	0.	0.	0.89893
1 H 10 – 0	0.00165	0.00099	0.	0.	0.84639
5 H 10 – 0	0.00824	0.00496	0.	0.	0.85695
20 H 10 – 0	0.03297	0.01982	0.	0.	0.89654
0 – 40 L 00	0.	0.	0.19471	0.	1.03846
0 – 200 L 00	0.	0.	0.97357	0.	1.81732
0 – 40 L 05	0.	0.	0.12300	0.06742	1.03417
0 – 200 L 05	0.	0.	0.61501	0.33709	1.79585
0 – 40 L 10	0.	0.	0.10413	0.08238	1.03026
0 – 200 L 10	0.	0.	0.52064	0.41191	1.77630
0 – 237 J 00	0.	0.	0.19894	0.	1.04269
0 – 1184 J 00	0.	0.	0.99469	0.	1.83844
0 – 234 J 05	0.	0.	0.14240	0.05159	1.03774
0 – 1172 J 05	0.	0.	0.71202	0.25794	1.81371
0 – 231 J 10	0.	0.	0.11806	0.07148	1.03329
0 – 1156 J 10	0.	0.	0.59031	0.35740	1.79145
20 H 05 – 200 L 05	0.04098	0.01420	0.61501	0.33709	1.85104
20 H 10 – 200 L 10	0.03297	0.01982	0.52064	0.41191	1.82909

TABLE XI. Values of various normal optical thicknesses at 0.3398 μm for the atmospheric models with 1,000 mb surface pressure and 0.250 atm-cm total ozone.

$\tau_b^{(s,R)} = 0.71800$ $\tau_b^{(a)} = 0.01205$

Aerosols	$\tau_b^{(s,ST)}$	$\tau_b^{(a,ST)}$	$\tau_b^{(s,TP)}$	$\tau_b^{(a,TP)}$	τ_b
1 H 00 - 0	0.00292	0.	0.	0.	0.73297
5 H 00 - 0	0.01458	0.	0.	0.	0.74463
20 H 00 - 0	0.05831	0.	0.	0.	0.78836
1 H 05 - 0	0.00206	0.00070	0.	0.	0.73281
5 H 05 - 0	0.01031	0.00350	0.	0.	0.74385
20 H 05 - 0	0.04123	0.01398	0.	0.	0.78526
1 H 10 - 0	0.00166	0.00098	0.	0.	0.73269
5 H 10 - 0	0.00829	0.00491	0.	0.	0.74325
20 H 10 - 0	0.03315	0.01963	0.	0.	0.78283
0 - 40 L 00	0.	0.	0.19550	0.	0.92555
0 - 200 L 00	0.	0.	0.97752	0.	1.70757
0 - 40 L 05	0.	0.	0.12410	0.06694	0.92109
0 - 200 L 05	0.	0.	0.62050	0.33468	1.68523
0 - 40 L 10	0.	0.	0.10481	0.08219	0.91704
0 - 200 L 10	0.	0.	0.52403	0.41093	1.66501
0 - 237 J 00	0.	0.	0.19550	0.	0.92555
0 - 1184 J 00	0.	0.	0.97751	0.	1.70756
0 - 234 J 05	0.	0.	0.14024	0.05080	0.92109
0 - 1172 J 05	0.	0.	0.70120	0.25398	1.68523
0 - 231 J 10	0.	0.	0.11639	0.07061	0.91704
0 - 1156 J 10	0.	0.	0.58193	0.35304	1.66501
20 H 05 - 200 L 05	0.04123	0.01398	0.62050	0.33468	1.74044
20 H 10 - 200 L 10	0.03315	0.01963	0.52403	0.41093	1.71779

TABLE XII. Values of various normal optical thicknesses at 0.3600 μm for the atmospheric models with 1,000 mb surface pressure and 0.250 atm-cm total ozone.

$\tau_b^{(s,R)} = 0.56340$ $\tau_b^{(a)} = 0.00030$

Aerosols	$\tau_b^{(s,ST)}$	$\tau_b^{(a,ST)}$	$\tau_b^{(s,TP)}$	$\tau_b^{(a,TP)}$	τ_b
1 H 00 – 0	0.00292	0.	0.	0.	0.56662
5 H 00 – 0	0.01459	0.	0.	0.	0.57829
20 H 00 – 0	0.05836	0.	0.	0.	0.62206
1 H 05 – 0	0.00208	0.00067	0.	0.	0.56646
5 H 05 – 0	0.01041	0.00337	0.	0.	0.57748
20 H 05 – 0	0.04164	0.01348	0.	0.	0.61882
1 H 10 – 0	0.00167	0.00096	0.	0.	0.56633
5 H 10 – 0	0.00836	0.00480	0.	0.	0.57686
20 H 10 – 0	0.03345	0.01919	0.	0.	0.61634
0 – 40 L 00	0.	0.	0.19722	0.	0.76092
0 – 200 L 00	0.	0.	0.98610	0.	1.54980
0 – 40 L 05	0.	0.	0.12655	0.06579	0.75605
0 – 200 L 05	0.	0.	0.63277	0.32897	1.52544
0 – 40 L 10	0.	0.	0.10633	0.08167	0.75170
0 – 200 L 10	0.	0.	0.53167	0.40835	1.50372
0 – 237 J 00	0.	0.	0.18762	0.	0.75132
0 – 1184 J 00	0.	0.	0.93812	0.	1.50182
0 – 234 J 05	0.	0.	0.13520	0.04900	0.74791
0 – 1172 J 05	0.	0.	0.67602	0.24502	1.48474
0 – 231 J 10	0.	0.	0.11246	0.06861	0.74477
0 – 1156 J 10	0.	0.	0.56230	0.34306	1.46906
20 H 05 – 200 L 05	0.04164	0.01348	0.63277	0.32897	1.58057
20 H 10 – 200 L 10	0.03345	0.01919	0.53167	0.40835	1.55636

TABLE XIII. Values of various normal optical thicknesses at 0.3800 μm for the atmospheric models with 1,000 mb surface pressure and 0.250 atm-cm total ozone.

$\tau_b^{(s,R)} = 0.44940$ $\tau_b^{(a)} = 0$

Aerosols	$\tau_b^{(s,ST)}$	$\tau_b^{(a,ST)}$	$\tau_b^{(s,TP)}$	$\tau_b^{(a,TP)}$	τ_b
1 H 00 – 0	0.00291	0.	0.	0.	0.45231
5 H 00 – 0	0.01453	0.	0.	0.	0.46393
20 H 00 – 0	0.05814	0.	0.	0.	0.50754
1 H 05 – 0	0.00209	0.00065	0.	0.	0.45214
5 H 05 – 0	0.01046	0.00325	0.	0.	0.46311
20 H 05 – 0	0.04184	0.01300	0.	0.	0.50424
1 H 10 – 0	0.00168	0.00094	0.	0.	0.45202
5 H 10 – 0	0.00840	0.00469	0.	0.	0.46249
20 H 10 – 0	0.03360	0.01875	0.	0.	0.50175
0 – 40 L 00	0.	0.	0.19872	0.	0.64812
0 – 200 L 00	0.	0.	0.99362	0.	1.44302
0 – 40 L 05	0.	0.	0.12881	0.06466	0.64287
0 – 200 L 05	0.	0.	0.64403	0.32330	1.41673
0 – 40 L 10	0.	0.	0.10775	0.08110	0.63824
0 – 200 L 10	0.	0.	0.53873	0.40549	1.39361
0 – 237 J 00	0.	0.	0.18017	0.	0.62957
0 – 1184 J 00	0.	0.	0.90086	0.	1.35026
0 – 234 J 05	0.	0.	0.13034	0.04733	0.62708
0 – 1172 J 05	0.	0.	0.65172	0.23665	1.33778
0 – 231 J 10	0.	0.	0.10865	0.06671	0.62476
0 – 1156 J 10	0.	0.	0.54324	0.33354	1.32618
20 H 05 – 200 L 05	0.04184	0.01300	0.64403	0.32330	1.47157
20 H 10 – 200 L 10	0.03360	0.01875	0.53873	0.40549	1.44596

by ozone at this wavelength. Values of the normal ozone-absorption optical thickness $[\tau_b^{(a)}]$ for the models with 0.450 atm-cm total ozone at λ = 0.3125, 0.3175, 0.3312, 0.3398, and 0.3600 are 0.75150, 0.40950, 0.07875, 0.02169, and 0.00054, respectively. A value of τ_b at a given wavelength and for a given model with 0.450 atm-cm total ozone can then be easily calculated after adding the difference between $\tau_b^{(a)}$ with 0.450 atm-cm and $\tau_b^{(a)}$ with 0.250 atm-cm, to the value of τ_b for the corresponding model with 0.250 atm-cm total ozone, and the appropriate wavelength.

IV. DISCUSSION OF RESULTS

4.1 *General:* Simulated measurements of the ultraviolet radiation backscattered by a column of the earth-atmosphere system along the local nadir, are analyzed in terms of the following quantities: *Effective Surface Albedo* ($\bar{R}$), *Best Ozone Estimate* (Ω_e) of the total ozone amount (Ω_{in}) in the column, and the *Improved Best Ozone Estimate* (Ω_e') which is determined after using information about the surface pressure (P_0) of the atmospheric model. Since all atmospheric models for which results are discussed in this report are for a surface pressure of 1,000 mb, the quantity $\Omega_e' = \Omega^I_{x,1000}$ which is the *improved total ozone amount* determined with the observations at the x-th wavelength pair, and 1,000 mb tables (see Sec. 1.3). Observations at the first wavelength pair (viz., 0.3312 - 0.3125 μm) are used for the determination $\Omega^I_{x,1000}$ if the solar zenith angle (θ_0) at the time and place of measurements is less than, or

equal to, 79.6°; observations at the second wavelength pair (viz., 0.3398 - 0.3175 μm) are used for measurements at higher values of θ_0.

Observations for the 5-wavelength, simulated BUV configuration are analyzed by making use of the SITC4 procedure. Those for the 6-wavelength, simulated configuration of the TOMS section of the SBUV/TOMS experiment are analyzed with the SITD1 procedure. A brief discussion of these total-ozone estimation procedures can be found in Sec. 1.3 of this report. A complete discussion of these procedures can be found in the Technical Report: II of this Contract (Dave, 1976 B). It will suffice to state here that the observations are analyzed in the SITC4 procedure (SITD1 procedure) by assuming that the reflectivity R of the surface underlying the model, and hence the *effective surface albedo* $\bar{R}$, are spectrally-independent (can be dependent upon the wavelength).

As mentioned in Sec. 3, results presented in this report are for atmospheric models resting on a surface whose Lambert reflectivity (R) is assumed to be independent of θ_0 and λ. However, because of the nature of the analytical procedures used, we find that the quantity $\bar{R}$ as obtained with the SITC4 procedure is a function of θ_0, and that obtained with the SITD1 procedure is a function θ_0 and also of λ.

4.2 *Physical Explanation:* The purpose of this report is to investigate the effect of atmospheric aerosols on the values of Ω_e (or Ω_e') determined by using the SITC4 and SITD1 procedures. However, a detailed physical explanation of a given observed effect is bound to be very

lengthy, and is likely to be meaningless, in many cases for several reasons. This is because of the basic nature of the total-ozone estimation procedures used.

First, the absolute measurements of the intensity of the back-scattered radiation at one or more wavelengths with insignificant absorption by ozone, are analyzed in terms of the pseudo-albedo values of the surface underlying the model. Hence, these pseudo-albedos are definitely dependent upon optical characteristics of aerosols in the model.

Second, values of the pseudo-albedos assigned to the wavelengths with significant absorption by ozone from those with insignificant absorption by it, are procedure dependent.

Third, the quantity used for the determination of Ω_e (or Ω_e') is the ratio of the measured intensities at two wavelengths of a given pair. This ratio is likely to be less dependent on aerosols than the corresponding pseudo-albedo values in many cases. On the other hand, the N_c vs. Ω_{in} curve (see Sec. 4.1 of Dave, 1976 B) used as a basis for getting Ω_e (or Ω_e') from the measured ratio of intensities may be significantly affected by errors in pseudo-albedos. Thus, even though the measured ratio of the intensities for the wavelength pair used to arrive at Ω_e (or Ω_e') may be unaffected by aerosols, the values of Ω_e (Ω_e') can significantly differ from the corresponding Ω_{in} due to errors in pseudo-albedo values. We can also encounter circumstances under which effects of aerosols on pseudo-albedos, and on the ratio of intensities in the regions of significant ozone absorption, are such that the net effect of aerosols on Ω_e (or Ω_e') is trivial.

Fourth, the change in Ω_e (or Ω_e') due to a given change in the magnitude of the ratio due to the presence of aerosols, is dependent upon θ_0, upon the wavelength pair, and also upon the slope of the N_c vs. Ω_{in} curve in the region of immediate interest.

Fifth, the final value of Ω_e (not of Ω_e') is arrived at after following different routes based on the magnitude of the ultimate *effective surface albedo* ($\bar{R}$). Presence of a given aerosol condition can lead to the following of a different route for the selection of Ω_e if the magnitude of $\bar{R}$ is significantly affected by these aerosol conditions.

From the discussion in the preceding paragraphs, it is clear that an explanation of an observed change in Ω_e (or Ω_e') due to a given atmospheric condition at the time of measurements, essentially involves tracing of various computational steps with actual numerical values. Such an explanation is not a real physical application. In fact, it can be considered as tedious, and to be of very little value. We have therefore considered it appropriate to hold our explanation of a given set of results, to a bare minimum level.

4.3 *Deviations* Δ *and* Δ'*:* In the last paragraph of Sec. 1.4, we mentioned that the effect of a given aerosol situation on the values of Ω_e and Ω_e' computed with either procedure will be investigated by presenting the values of the *deviation* Δ [$= 1{,}000 \times (\Omega_e - \Omega_{in})$], and the *deviation* Δ' [$= 1{,}000 \times (\Omega_e' - \Omega_{in})$]. We will now compare the values of Δ and Δ' for a few selected cases to see advantages of carrying out investigations of

the effect of aerosols on total-ozone estimations with the *deviation* Δ', rather than with the *deviation* Δ. It should be pointed out that the current, NASA total-ozone estimation procedure for the BUV data is strictly for the evaluation of the quantity Ω_e, and hence the *deviation* Δ is more useful than the *deviation* Δ', at this time. However, there are plans for the evaluation of the quantity Ω_e' in the near future. In the meanwhile, investigations using the *deviation* Δ' are for the purposes of obtaining a very clear understanding of the effect of aerosols on the values of total ozone estimated from the analysis of the radiation back-scattered by the earth-atmosphere system.

In Table XIV, we have given values of Δ and Δ' for three different atmospheric models (viz., 20 H 00 - 0, 5 H 05 - 0, and 20 H 05 - 0) with Ω_{in} = 0.250 atm-cm. These values obtained with the SITC4 procedure are tabulated for two values of the Lambert reflectivity (R = 0.1 and 0.8) of the surface underlying the models, and for ten different values of the solar zenith angle (θ_0). For the cases with R = 0.1, the presence of the stratospheric aerosols in the models affects the values of Ω_e or Ω_e' in an insignificant manner for $\theta_0 \leq 84.7°$. Furthermore, the *deviations* Δ and Δ' are equal for all cases for which the results are presented in the upper part of Table XIV. On the other hand, values of Δ given in the lower section of Table XIV for the models resting on a surface with R = 0.8, differ very significantly from those of Δ' for all cases with $\theta_0 \leq 79.6°$. A comparison of the values of Δ' for various cases suggests that the presence of a strongly reflecting surface underneath a

TABLE XIV. Comparison of the *deviations* Δ and Δ' for a few selected atmospheric models with stratospheric aerosols.

Ω_{in} = 0.250 atm-cm P_0 = 1,000 mb

Procedure: SITC4

θ_0	20 H 00 – 0		5 H 05 – 0		20 H 05 – 0	
	Δ	Δ'	Δ	Δ'	Δ	Δ'
			R = 0.1			
0.0	-2	-2	1	1	3	3
45.0	1	1	1	1	3	3
60.0	1	1	1	1	3	3
70.0	1	1	1	1	3	3
75.6	0	0	1	1	3	3
79.6	-1	-1	0	0	1	1
82.5	-1	-1	1	1	4	4
84.7	-3	-3	0	0	-1	-1
86.7	-8	-8	-2	-2	-8	-8
90.0	-51	-51	-17	-17	-53	-53
			R = 0.8			
0.0	24	1	24	0	24	2
45.0	22	1	20	0	20	2
60.0	18	1	16	0	16	2
70.0	13	1	12	0	12	2
75.6	9	0	9	0	9	1
79.6	6	-1	8	0	6	0
82.5	4	-1	5	0	3	0
84.7	0	-4	4	-1	-2	-4
86.7	-5	-8	1	-3	-10	-11
90.0	-48	-49	-14	-18	-61	-60

model, tends to diminish slightly the effect of stratospheric aerosols on total-ozone estimates, for $\theta_0 \leq 79.6°$. It would be rather difficult to arrive at such a conclusion from the examination of data for the *deviation* Δ.

Values of Δ and Δ' for three different atmospheric models with tropospheric aerosols (viz., 0 - 200 L 00, 0 - 40 L 05, and 0 - 200 L 05) as obtained with the SITC4 and SITD1 procedures are given in Tables XV and XVI, respectively. These results are also for $\Omega_{in} = 0.250$ atm-cm, $P_0 = 1{,}000$ mb, R = 0.0 and 0.1, and 10 different values of θ_0 given in Table XIV. As the tropospheric aerosol material is changed from a non-absorbing one (model: 0 - 200 L 00) to a partly-absorbing one (model: 0 - 200 L 05), values of the *deviation* Δ as obtained with the SITC4 procedure generally show an increase at all θ_0 for R = 0.1, but a decrease at all θ_0 for R = 0.8. On the other hand, corresponding values of the *deviation* Δ' generally show an increase with an increase of the parameter n_2 from 0.00 to 0.05, for both values of R. Similar trends can also be seen as the tropospheric aerosol content is increased from 40 to 200 million particles (from the model 0 - 40 L 05, to the model 0 - 200 L 05). Thus, it can be seen that the *deviation* Δ' is a better choice for studying the effect of aerosols on total-ozone estimates, than the *deviation* Δ. This is primarily because errors introduced in Ω_e due to the absence of any information about the surface pressure at the place and time of observation, are comparable to those due to the presence of aerosols in the atmosphere.

TABLE XV. Comparison of the *deviations* Δ and Δ' for a few selected atmospheric models with tropospheric aerosols.

Ω_{in} = 0.250 atm-cm P_0 = 1,000 mb

Procedure: SITC4

θ_0	0 - 200 L 00		0 - 40 L 05		0 - 200 L 05	
	Δ	Δ'	Δ	Δ'	Δ	Δ'
			R = 0.1			
0.0	-2	-1	2	2	7	7
45.0	-2	-1	2	2	6	6
60.0	-1	0	1	1	5	5
70.0	0	0	1	1	3	3
75.6	0	0	0	0	2	2
79.6	0	0	0	0	1	1
82.5	-1	0	1	1	2	2
84.7	-1	0	1	1	2	2
86.7	-1	-1	1	1	2	2
90.0	-3	-2	3	3	11	11
			R = 0.8			
0.0	25	1	16	2	8	8
45.0	20	0	12	1	6	6
60.0	15	-1	9	1	3	4
70.0	11	-1	6	0	2	2
75.6	9	0	4	0	1	1
79.6	8	0	4	0	1	0
82.5	5	-1	3	0	1	2
84.7	5	-1	3	0	1	1
86.7	6	-1	3	0	1	1
90.0	11	-2	7	1	6	7

TABLE XVI. Comparison of the *deviations* Δ and Δ' for a few selected atmospheric models with tropospheric aerosols.

Ω_{in} = 0.250 atm-cm P_0 = 1,000 mb

Procedure: SITD1

θ_0	0 - 200 L 00		0 - 40 L 05		0 - 200 L 05	
	Δ	Δ'	Δ	Δ'	Δ	Δ'
			R = 0.1			
0.0	1	-1	0	0	1	1
45.0	2	0	0	0	1	1
60.0	2	0	0	0	1	1
70.0	2	0	0	0	0	0
75.6	1	0	0	0	0	0
79.6	1	0	0	0	0	0
82.5	1	0	0	0	0	0
84.7	1	0	0	0	0	0
86.7	0	0	0	0	0	0
90.0	3	0	-1	-1	-1	-1
			R = 0.8			
0.0	22	-1	14	-1	1	-1
45.0	21	0	12	-1	1	0
60.0	18	0	10	0	1	0
70.0	14	0	8	0	1	0
75.6	11	0	6	0	0	0
79.6	9	0	5	0	0	0
82.5	8	0	4	0	0	0
84.7	7	0	4	0	0	0
86.7	8	0	4	-1	0	-1
90.0	28	0	15	-2	0	-2

4.4 *Effect of the Stratospheric Aerosols:* Values of the *deviation* Δ' for the atmospheric models with only stratospheric aerosols are presented in Tables XVII through XX for a total input ozone amount of 0.250 atm-cm. Results obtained with the SITC4 (SITD1) procedure are given in Tables XVII and XVIII (XIX and XX) for R = 0.1 and 0.8, respectively. In each table, results in the first row are for a model with no aerosols (0 - 0). Rows 2 - 4, 5 - 7, and 8 - 10 contain values of Δ' (for 10 different values of θ_0 listed earlier) for the stratospheric aerosol material with m = 1.5 - 0.00i, 1.5 - 0.05i, and 1.5 - 0.10i, respectively. The total stratospheric aerosol content increases from 1 to 5, to 20 × 10^6 particles (size-distribution function: *Haze H*) as we move downward in a given set of three rows for a fixed value of the parameter m.

In a real terrestrial atmosphere, stratospheric aerosol contents greater than 20 million particles may be encountered due to natural or human causes such as volcanic eruptions and high-altitude explosions. However, we feel that a stratospheric aerosol content of 20 × 10^6 is very high for average atmospheric conditions for several reasons. Let us consider the total normal optical thicknesses at 0 km level due to aerosols, and due to molecules for the model 20 H 00 - 0 at λ = 0.3800 μm. From the Table XIII, we find that $\tau_b^{(s,R)} = 0.449$ and $\tau_b^{(s,ST)} = 0.058$. However, since almost all stratospheric aerosol particles are assigned to parts of the atmosphere located above 15 km, it is more meaningful to compare values of $\tau^{(s,R)}$ and $\tau^{(s,ST)}$ at 16 km level. At this level, $\tau^{(s,R)} \doteqdot 0.04$ and $\tau^{(s,ST)} \doteqdot 0.06$, i.e., aerosol and molecular normal

TABLE XVII. Values of the *deviation* Δ' [$= 1{,}000 \times (\Omega_e' - \Omega_{in})$] for the atmospheric models with $\Omega_{in} = 0.250$ atm-cm and stratospheric aerosols; $P_0 = 1{,}000$ mb.

Procedure: SITC4 R = 0.1

Aerosols	Δ' for θ_0 =									
	0.0	45.0	60.0	70.0	75.6	79.6	82.5	84.7	86.7	90.0
0 - 0	0	0	0	0	0	0	0	0	0	0
1 H 00 - 0	0	0	0	0	0	0	0	0	0	-3
5 H 00 - 0	0	0	0	0	0	0	0	-1	-2	-15
20 H 00 - 0	-2	1	1	1	0	-1	-1	-3	-8	-51
1 H 05 - 0	0	0	0	0	0	0	0	0	0	-4
5 H 05 - 0	1	1	1	1	1	0	1	0	-2	-17
20 H 05 - 0	3	3	3	3	3	1	4	-1	-8	-53
1 H 10 - 0	0	0	0	0	0	0	0	0	0	-4
5 H 10 - 0	1	1	1	1	1	1	1	0	-2	-17
20 H 10 - 0	4	4	4	4	4	2	5	1	-7	-54

TABLE XVIII. Values of the *deviation* Δ' [= $1{,}000 \times (\Omega_e' - \Omega_{in})$] for the atmospheric models with Ω_{in} = 0.250 atm-cm and stratospheric aerosols; P_0 = 1,000 mb.

Procedure: SITC4 R = 0.8

Aerosols	Δ' for θ_0 =									
	0.0	45.0	60.0	70.0	75.6	79.6	82.5	84.7	86.7	90.0
0 - 0	0	0	0	0	0	0	0	0	0	0
1 H 00 - 0	0	0	0	0	0	0	0	0	0	-3
5 H 00 - 0	0	0	0	0	0	0	0	-1	-2	-14
20 H 00 - 0	1	1	1	1	0	-1	-1	-4	-8	-49
1 H 05 - 0	0	0	0	0	0	0	0	0	-1	-4
5 H 05 - 0	0	0	0	0	0	0	0	-1	-3	-18
20 H 05 - 0	2	2	2	2	1	0	0	-4	-11	-60
1 H 10 - 0	0	0	0	0	0	0	0	0	-1	-4
5 H 10 - 0	0	0	1	1	0	0	0	-1	-3	-20
20 H 10 - 0	2	2	2	2	2	0	0	-4	-12	-64

TABLE XIX. Values of the *deviation* Δ' $[= 1{,}000 \times (\Omega_e' - \Omega_{in})]$ for the atmospheric models with Ω_{in} = 0.250 atm-cm and stratospheric aerosols; P_0 = 1,000 mb.

Procedure: SITD1 R = 0.1

Aerosols	Δ' for θ_0 =									
	0.0	45.0	60.0	70.0	75.6	79.6	82.5	84.7	86.7	90.0
0 - 0	0	0	0	0	0	0	0	0	0	0
1 H 00 - 0	0	0	0	0	0	0	0	0	-1	-5
5 H 00 - 0	0	0	0	0	0	0	0	-1	-3	-20
20 H 00 - 0	-1	1	1	0	0	-2	-2	-4	-10	-68
1 H 05 - 0	0	0	0	0	0	0	0	0	-1	-5
5 H 05 - 0	0	0	0	0	0	0	0	-1	-3	-24
20 H 05 - 0	1	1	1	1	1	-1	-1	-5	-13	-82
1 H 10 - 0	0	0	0	0	0	0	0	0	-1	-6
5 H 10 - 0	0	0	0	0	0	0	0	-1	-4	-25
20 H 10 - 0	1	1	2	2	1	0	-1	-5	-13	-86

TABLE XX. Values of the *deviation* Δ' $[= 1{,}000 \times (\Omega_e' - \Omega_{in})]$ for the atmospheric models with Ω_{in} = 0.250 atm-cm and stratospheric aerosols; P_0 = 1,000 mb.

Procedure: SITD1 R = 0.8

Aerosols	Δ' for θ_0 =									
	0.0	45.0	60.0	70.0	75.6	79.6	82.5	84.7	86.7	90.0
0 - 0	0	0	0	0	0	0	0	0	0	0
1 H 00 - 0	0	0	0	0	0	0	0	0	0	-4
5 H 00 - 0	0	0	0	0	0	0	0	-1	-2	-16
20 H 00 - 0	1	1	1	1	0	-1	-1	-4	-8	-52
1 H 05 - 0	0	0	0	0	0	0	0	0	-1	-4
5 H 05 - 0	0	0	0	0	0	0	0	-1	-3	-19
20 H 05 - 0	1	1	1	1	1	-1	-2	-5	-12	-65
1 H 10 - 0	0	0	0	0	0	0	0	0	-1	-5
5 H 10 - 0	0	0	0	0	0	0	0	-1	-3	-20
20 H 10 - 0	1	1	1	1	1	0	-2	-5	-13	-69

optical thicknesses at 0.3800 μm wavelength for the 20 H 00 - 0 model are practically equal at about 16 km level. This is because, for this model, most of the molecules are situated below this level, while most of the aerosols are situated above this level. Since the molecular (or Rayleigh) optical thickness is inversely proportional to the fourth power of the wavelength but the aerosol optical thickness shows only a mild dependence on wavelength (Fig. 2), the ratio of the aerosol to Rayleigh optical thickness at 16 km for the 20 H 00 - 0 model will increase from about unity at $\lambda = 0.3800$ μm, to about 5 at 0.6 μm. This is a very large ratio indeed. Dave and Mateer (1968) have shown that such a high stratospheric contamination leads to the occurrence of bright purple twilights which are only observed after very powerful volcanic eruptions. We therefore feel that the average stratospheric aerosol conditions are better represented by 5 H mm molds.

The following observations are made after studying the data presented in Tables XVII through XX:

(i) The presence of a variety of stratospheric aerosol conditions leads to an over-estimation of total ozone by a very small amount (highest values of Δ' observed is about 4 units for the 20 H 10 model with $R = 0.1$ when the SITC4 procedure is used; Table XVII), when the solar zenith angle at the time of simulated measurements is less than 80°.

(ii) For $\theta_0 > 80°$, the presence of stratospheric aerosols leads to a significant under-estimation of the total ozone in the atmospheric

column underneath the satellite. The degree of this underestimation increases with an increase of θ_0, and also with an increase of the aerosol content. As for example, for the $R = 0.1$, $\theta_0 = 90°$ case of the model 20 H 05 – 0, the SITC4 procedure yields a value of -53 units for Δ', i.e., we have underestimated total ozone by about 20% under these conditions.

(iii) For $\theta_0 < 80°$, values of Δ' obtained with the SITD1 procedure are generally smaller than those for the corresponding cases obtained with the SITC4 procedure. As for example, for the case $\theta_0 = 0°$, $R = 0.1$ of the 20 H 10 – 0 model, Δ' as obtained with the SITC4 and SITD1 procedures carries a value of 4 and 1 units, respectively.

(iv) An increase in the imaginary part (n_2) of the refractive index of the aerosol material from 0.00 to 0.10 lead to only small changes in Δ' when the sun is not near the local horizon. For $\theta_0 = 90°$, some dependence of Δ' on n_2 is noticeable.

(v) Especially for the high values of θ_0, the changes in Δ' with increase in the value of the surface reflectivity are, to some extent, procedure-dependent.

In order to obtain some understanding of the dependence of Δ' on θ_0 discussed under (i) and (ii) above, we will denote the ratio of the intensity at the wavelength λ of the radiation back-scattered by the model nn H mm – 0, to that back-scattered by the model 0 – 0, by the symbol

$\rho_{st}(\lambda, \theta_0, \text{nn H mm} - 0)$. The parameters Ω_{in}, θ, R, and P_0 are suppressed for brevity. Variations of $\rho_{st}(\lambda, \theta_0, \text{nn H mm} - 0)$ vs. λ for $\theta_0 = 0°$, 79.6°, and 90°, and for the atmospheric models 20 H 00 - 0, 20 H 05 - 0, and 20 H 10 - 0 are shown in Fig. 6.

For $\theta_0 = 0°$, the quantity $\rho_{st}(\lambda, \theta_0, \text{nn H mm} - 0)$ is independent of λ for all practical purposes. This is because almost all of the emergent radiation originates from below the stratospheric aerosol layer for this case of the overhead sun. The stratospheric aerosol layer primarily acts as an additional attenuator to the incoming solar, and the outgoing planetary radiations. However, this is not strictly true as the ratio $\rho_{st}(\lambda, 0°, 20\text{ H }00 - 0) \doteqdot 1.03$ suggesting that there is some contribution to the outgoing radiation by the nonabsorbing aerosols in the model. An increase in the imaginary part of the refractive index of the aerosol material from 0.00 (Model 20 H 00 - 0), to 0.05 (Model 20 H 05 - 0), to 0.10 (Model 20 H 10 - 0) results in the lowering of $\rho_{st}(\lambda, \theta_0, 20\text{ H mm} - 0)$ from 1.03, to 0.98, to 0.96. If we now go through various steps of the total-ozone estimation procedure (see Sec. 4.2), we will find some changes in pseudo-albedo values, but very little change in the ratio of intensities for either wavelength pair. Thus, a weak dependence of Δ' on n_2 seen in the results presented for $\theta_0 = 0°$ in Table XVII can be attributed to shifts of the N_c vs. Ω_{in} curves due to the changes in pseudo-albedo values. It is interesting to note that this weak dependence of Δ' on n_2 decreases with increase of the parameter R and also as we go from the SITC4 to SITD1 procedure.

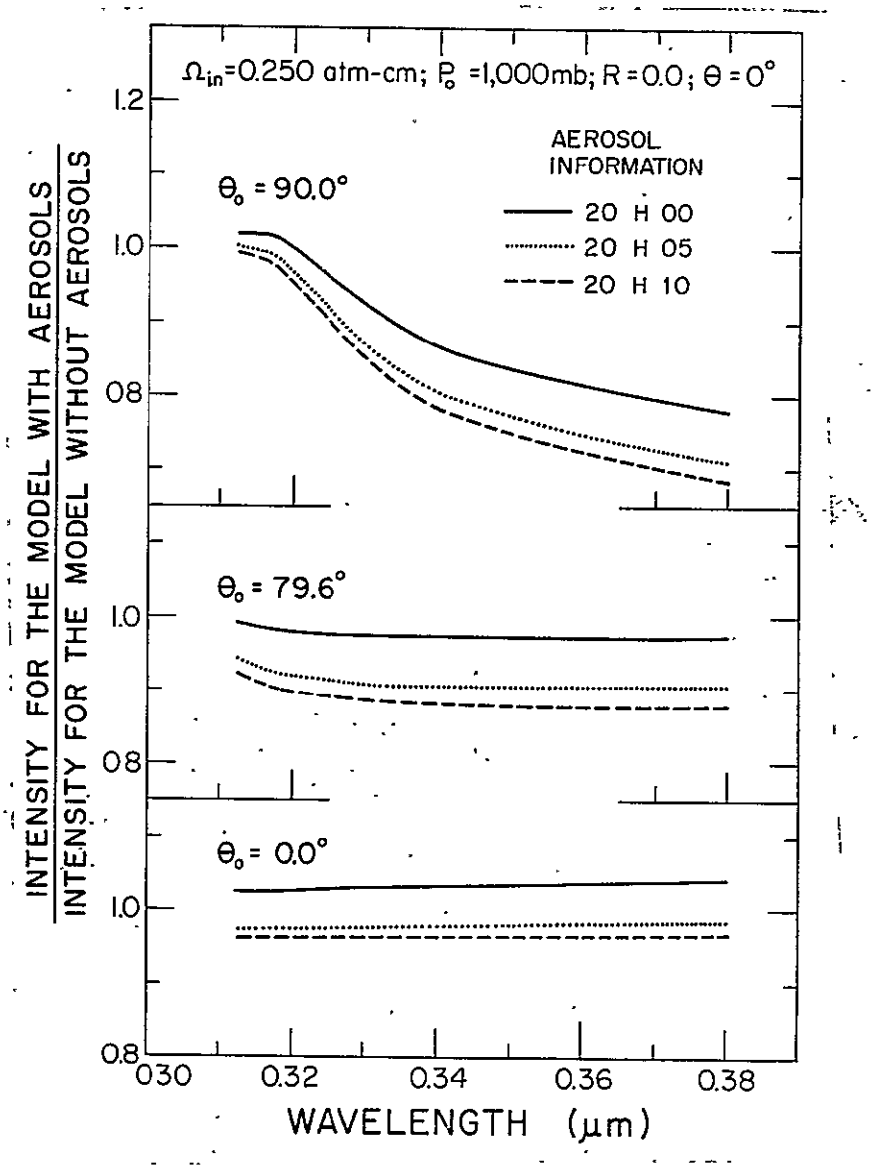

Fig. 6. Variations, as a function of the wavelength (μm), of the changes in the intensity of radiation emerging along the nadir direction ($\theta = 0°$) due to the presence of stratospheric aerosols (Total amount: 20×10^6 particles; Size distribution: *Haze H*) in the atmospheric model. $\Omega_{in} = 0.250$ atm-cm; $P_0 = 1{,}000$ mb; R = 0.0. Solid curve: m = 1.5 - 0.0i; Dotted curve: m = 1.5 - 0.05i; Broken curve: m = 1.5 - 0.10i.

For $\theta_0 = 79.6°$, there is some dependence of the ratio $\rho_{st}(\lambda, \theta_0,$ nn H mm − 0) on λ at shorter wavelengths. However, the overall effect of the aerosol layer is now that of an attenuator in all three cases.

For $\theta_0 = 90°$, the ratio $\rho_{st}(\lambda, 90°,$ nn H mm − 0) decreases very rapidly with an increase of λ from 0.3175 μm to 0.3398 μm. This is because the scattered radiation in the 0.3100 − 0.3200 μm region originates from the parts of the atmosphere located above the aerosol layer, while that in the 0.3200 − 0.3400 μm region originates from the parts of the atmosphere located within and under the aerosol layer. This strong dependence of $\rho_{st}(\lambda, \theta_0,$ nn H mm − 0) on λ results in the under-estimation of the pseudo-albedo values used in the generation of the N_c vs. Ω_{in} curves used in the estimation of ozone, and also of the ratio of the measured intensities at the second wavelength pair. The net result of this under-estimation at two stages is a very significant under-estimation of the total ozone by the procedure.

In Tables XXI and XXII, we have presented values of the *deviation* Δ' in the format identical to that of Tables XVII through XX, but for $\Omega_{in} = 0.450$ atm-cm. Values of Δ' obtained with the SITC4 and SITD1 procedures for models resting on a surface with a Lambert reflectivity (R) of 0.8 are given in Tables XXI and XXII, respectively.

A comparison of the results presented in Table XXI with those presented in Table XVIII (and those presented in Table XXII with those presented in Table XX) suggests that the effect of a stratospheric aerosol layer of a given characteristic on the estimate of total ozone is more

TABLE XXI. Values of the *deviation* Δ' [$= 1{,}000 \times (\Omega_e' - \Omega_{in})$] for the atmospheric models with Ω_{in} = 0.450 atm-cm, and stratospheric aerosols; P_0 = 1,000 mb.

Procedure: SITC4 R = 0.8

Aerosols	Δ' for θ_0 =									
	0.0	45.0	60.0	70.0	75.6	79.6	82.5	84.7	86.7	90.0
0 - 0	0	0	0	0	0	0	0	0	0	0
1 H 00 - 0	0	0	0	0	0	-1	-1	-1	-2	-5
5 H 00 - 0	0	1	0	-1	-2	-5	-4	-7	-12	-29
20 H 00 - 0	0	2	1	-3	-9	-19	-18	-29	-46	-
1 H 05 - 0	0	0	0	0	0	-1	-1	-1	-3	-7
5 H 05 - 0	1	1	1	0	-1	-3	-3	-7	-14	-37
20 H 05 - 0	3	3	3	1	-3	-11	-12	-26	-52	-
1 H 10 - 0	0	0	0	0	0	0	0	-1	-3	-8
5 H 10 - 0	1	1	1	1	0	-2	-2	-6	-14	-40
20 H 10 - 0	3	3	3	2	-1	-8	-9	-24	-54	-

TABLE XXII. Values of the *deviation* Δ' [$= 1{,}000 \times (\Omega_e' - \Omega_{in})$] for the atmospheric models with $\Omega_{in} = 0.450$ atm-cm and stratospheric aerosols; $P_0 = 1{,}000$ mb.

Procedure: SITD1 R = 0.8

Aerosols	Δ' for θ_0 =									
	0.0	45.0	60.0	70.0	75.6	79.6	82.5	84.7	86.7	90.0
0 - 0	0	0	0	0	0	0	0	0	0	0
1 H 00 - 0	0	0	0	0	0	-1	-1	-2	-3	-4
5 H 00 - 0	0	0	0	-1	-2	-5	-5	-8	-13	-19
20 H 00 - 0	0	2	0	-3	-9	-19	-19	-30	-50	-57
1 H 05 - 0	0	0	0	0	0	-1	-1	-2	-3	-5
5 H 05 - 0	1	1	0	0	-1	-3	-4	-7	-15	-23
20 H 05 - 0	2	2	2	0	-4	-11	-14	-30	-57	-75
1 H 10 - 0	0	0	0	0	0	0	-1	-1	-3	-5
5 H 10 - 0	1	1	1	0	0	-2	-3	-7	-16	-24
20 H 10 - 0	2	2	2	1	-1	-8	-12	-29	-60	-82

pronounced at Ω_{in} = 0.450 atm-cm, than at Ω_{in} = 0.250 atm-cm, especially when the sun is near the local horizon. As for example, for the case R = 0.8, θ_0 = 79.6° of the model 20 H 00 - 0, the *deviation* Δ' as obtained with either procedure carries a value of -1 unit when Ω_{in} = 0.250 atm-cm, but a value of -19 units when Ω_{in} = 0.450 atm-cm. It is clear that a significant underestimation of the total ozone occurring only at very low sun positions ($\theta_0 \geq 86.7°$) for the low ozone amount cases, is evident even at θ_0 = 75.6° for the moderate ozone amount cases. Furthermore, the change in Δ' with aerosol parameter n_2 is also strongly dependent upon θ_0. As for example, the *deviation* Δ' = -19, -11, and -8 units at θ_0 = 79.6° for the models 20 H 00 - 0, 20 H 05 - 0, and 20 H 10 - 0, respectively, but is equal to -46, -52, and -54 at θ_0 = 86.7° for the respective models (see Table XXI).

In order to understand the reasons behind an increase in the underestimation of the total ozone with an increase in Ω_{in} at large values of θ_0 discussed in the preceding paragraph, we will examine the values of $\rho_{st}(\lambda, 79.6°, 20\,H\,00 - 0)$ at all six wavelengths for the models with different ozone amounts. For the model with Ω_{in} = 0.250 atm-cm, $\rho_{st}(\lambda, 79.6°, 20\,H\,00 - 0)$ = 0.993, 0.981, 0.974, 0.973, 0.971, and 0.972 for λ = 0.3125, 0.3175, 0.3312, 0.3398, 0.3600, and 0.3800 μm, respectively. For the model with Ω_{in} = 0.450 atm-cm, this ratio carries a value of 1.032, 1.014, 0.980, 0.974, 0.971, and 0.972, respectively. Thus, an increase in ozone amount (Ω_{in}) cannot result in any change in the pseudo-albedo values used in the generation of the N_c vs. Ω_{in}.

curves required for the estimation of total ozone. Thus, these basic N_c vs. Ω_{in} curves do not shift as we increase the total ozone content from 0.250 to 0.450 atm-cm, keeping the aerosol properties unchanged. The ratio of the measured intensities for both wavelength pairs does decrease by a small amount, but this decrease is too small to explain the observed under-estimation of total ozone. It is clear that the real reason behind the observed increase in the degree of under-estimation of total ozone with increase in Ω_{in} from 0.250 to 0.450 atm-cm, is the decrease in the slope of the N_c vs. Ω_{in} curve with an increase in Ω_{in} (see Fig. 1 of Dave, 1976 B).

From the discussion in the preceding paragraphs, it can be concluded that the current analytic procedures can yield significantly lower estimates of total ozone in an atmospheric column if the measurements are taken at solar zenith angles exceeding 75°, if the actual total ozone content of the column is moderate to high, and if the stratospheric particulate contaminants are also at moderate to high levels. Naturally, the degree of under-estimation depends upon all these and several other factors such as the reflectivity of the surface underlying the column. These findings warrant a critical examination of the seasonal and geographical variations of the aerosol content of the 15 - 50 km region on a global scale, and its comparison with the stratospheric aerosol data used in the investigations reported in this section.

4.5 *Effect of the Tropospheric Aerosols:* Values of the *deviation* Δ' for the atmospheric models with only tropspheric aerosols are presented in

Tables XXIII and XXIV for a value of 0.1 and 0.8, respectively, of the Lambert reflectivity (R) of the surface underlying the atmospheric models. Results given in these tables are for a total atmospheric ozone content (Ω_{in}) of 0.250 atm-cm. Values of Δ' obtained with the SITC4 (SITD1) procedure are given in the upper (lower) section of these tables. Each section consists of seven rows with each row containing values of Δ' for 10 different values of θ_0 listed earlier. The top-most row of a section provides results for an aerosol-free atmospheric model (0 - 0). Row 2 - 3, 4 - 5, and 6 - 7 contain values of Δ' for the tropospheric aerosol material with $m = 1.5 - 0.00i$, $1.5 - 0.05i$, and $1.5 - 0.10i$, respectively, with the upper (lower) row of a group representing results for 40 (200) million tropospheric aerosol particles in a column. Results presented in these two tables are for the existence of the tropospheric aerosols in the form of a spherical polydispersion whose size-distribution function is designated *Haze L* (see Sec. 2.1).

The total normal optical thickness due to Rayleigh scattering $[\tau_b^{(s,R)}]$ of a terrestrial atmosphere with 1,000 mb surface pressure, is about 0.45 at 0.3800 μm (see Table XIII). From the same Table, we also find that the total normal optical thicknesses due to the tropospheric aerosol scattering $[\tau_b^{(s,TP)}]$ are 0.20 and 0.99 for the models 0 - 40 L 00, and 0 - 200 L 00, respectively. However, values of the atmospheric turbidity are generally expressed in terms of the ratio of $\tau_b^{(s,TP)}$ to $\tau_b^{(s,R)}$ at about 0.55 μm. The value of $\tau_b^{(s,R)} \doteq 0.1$ at 0.55 μm. From Fig. 2, we find that the quantity $\tau_b^{(s,TP)}$ increases with λ for the *Haze L* in

TABLE XXIII. Values of the *deviation* Δ' [$= 1{,}000 \times (\Omega_e' - \Omega_{in})$] for the atmospheric models with $\Omega_{in} = 0.250$ atm-cm and tropospheric aerosols; $P_0 = 1{,}000$ mb; $R = 0.1$.

Aerosols	Δ' for θ_0 =									
	0.0	45.0	60.0	70.0	75.6	79.6	82.5	84.7	86.7	90.0
Procedure: SITC4										
0 - 0	0	0	0	0	0	0	0	0	0	0
0 - 40 L 00	0	0	0	0	0	0	0	0	0	0
0 - 200 L 00	-1	-1	0	0	0	0	0	0	-1	-2
0 - 40 L 05	2	2	1	1	0	0	1	1	1	3
0 - 200 L 05	7	6	5	3	2	1	2	2	2	11
0 - 40 L 10	2	2	1	1	0	0	1	1	1	3
0 - 200 L 10	8	7	5	3	2	1	3	2	2	12
Procedure: SITD1										
0 - 0	0	0	0	0	0	0	0	0	0	0
0 - 40 L 00	0	0	0	0	0	0	0	0	0	-1
0 - 200 L 00	-1	0	0	0	0	0	0	0	0	0
0 - 40 L 05	0	0	0	0	0	0	0	0	0	-1
0 - 200 L 05	1	1	1	0	0	0	0	0	0	-1
0 - 40 L 10	0	0	0	0	0	0	0	0	0	-1
0 - 200 L 10	2	1	1	0	0	0	0	0	0	-1

TABLE XXIV. Values of the *deviation* Δ' $[= 1{,}000 \times (\Omega_e' - \Omega_{in})]$ for the atmospheric models with Ω_{in} = 0.250 atm-cm, and tropospheric aerosols; P_0 = 1,000 mb; R = 0.8.

Aerosols	Δ' for θ_0 =									
	0.0	45.0	60.0	70.0	75.6	79.6	82.5	84.7	86.7	90.0
Procedure: SITC4										
0 - 0	0	0	0	0	0	0	0	0	0	0
0 - 40 L 00	0	0	0	0	0	0	0	0	0	-1
0 - 200 L 00	1	0	-1	-1	0	0	-1	-1	-1	-2
0 - 40 L 05	2	1	1	0	0	0	0	0	0	1
0 - 200 L 05	8	6	4	2	1	0	2	1	1	7
0 - 40 L 10	2	1	0	0	0	0	-1	0	0	0
0 - 200 L 10	9	7	4	2	1	0	1	1	1	8
Procedure: SITD1										
0 - 0	0	0	0	0	0	0	0	0	0	0
0 - 40 L 00	0	0	0	0	0	0	0	0	0	-1
0 - 200 L 00	-1	0	0	0	0	0	0	0	0	0
0 - 40 L 05	-1	-1	0	0	0	0	0	0	-1	-2
0 - 200 L 05	-1	0	0	0	0	0	0	0	-1	-2
0 - 40 L 10	-1	-1	0	0	0	0	0	0	-1	-2
0 - 200 L 10	0	0	0	0	0	0	0	0	-1	-1

the spectral range 0.31 - 0.38 μm. From Braslau and Dave (1973), we find that from this case, $\tau_b^{(s,TP)}$ continues to increase with an increase of λ up to 0.55 μm. Thus, the turbidity factor [i.e., the ratio $\tau_b^{(s,TP)}/\tau_b^{(s,R)}$] is about 2 - 2.5 for the model 0 - 40 L 00, and is about 10 - 12.5 for the model 0 - 200 L 00. Based on this data, we feel that our 0 - 40 L mm models represent average aerosol conditions and 0 - 200 L mm models represent strong hazy conditions. However, it should be pointed out that atmospheric conditions can be encountered under which the turbidity factors would be greater than the ones used in our investigations.

An examination of the results presented in Tables XXIII and XXIV brings out the following:

(i) Even the presence of large tropospheric aerosol content has very insignificant effect ($\Delta' = -2$) on the estimated values of the total ozone, provided the aerosol material is a nonabsorbing one (model: 0 - 200 L 00).

(ii) The presence of a large amount of partly-absorbing aerosols in the troposphere (model 0 - 200 L 05 and 0 - 200 L 10) results in an over-estimation of total ozone in the atmospheric column by about 8 to 12 units, only when the sun is very near the local zenith, or very near the local horizon. Furthermore, this over-estimation occurs only if the SITC4 procedure is used for the analysis of measurements.

(iii) The effect of the tropospheric aerosols on total ozone estimates as obtained with the SITC4 procedure, is the smallest at $\theta_0 = 79.6°$.

(iv) Values of Ω_e' as obtained with the SITD1 procedure are very insensitive to the aerosols in the lower troposphere.

In Fig. 7, we have plotted values of the ratio $\rho_{th}(\lambda, \theta_0, 0-nn\,L\,mm)$ as a function of the wavelength λ for $\theta_0 = 0°$, 79.6°, and 90°, and for the atmospheric models 0 - 200 L 00, 0 - 200 L 05, and 0 - 200 L 10. This ratio represents the intensity at the wavelength λ of the radiation back-scattered by the model 0 - nn L mm, to that back-scattered by the model 0 - 0. The parameters Ω_{in}, P_0, R, and θ which are common to both cases, are suppressed for brevity. The ratio $\rho_{th}(\lambda, 0°, 0-200\,L\,00)$ increases very rapidly with an increase of λ. However, such a strong effect of aerosols on the individual intensity measurements has very little effect ($\Delta' = -1$ and 1 for $R = 0.1$ and 0.8, respectively; see Tables XXIII and XXIV) on Ω_e'. On the other hand, a relatively weak dependence of $\rho_{th}(\lambda, 0°, 0-200\,L\,05)$ and $\rho_{th}(\lambda, 0°, 0-200\,L\,10)$ on λ results in a relatively strong effect on Ω_e'. There are only minor differences between $\rho_{th}(\lambda, 79.6°, 0-200\,L\,mm)$ vs. λ, and $\rho_{th}(\lambda, 90°, 0-200\,L\,mm)$ vs. λ curves. However, the effects of these changes in intensities on the corresponding values of Ω_e' are significantly different.

The strong procedure dependence of the effect of tropospheric aerosols on Ω_e' can be explained as follows: Since aerosols are very near

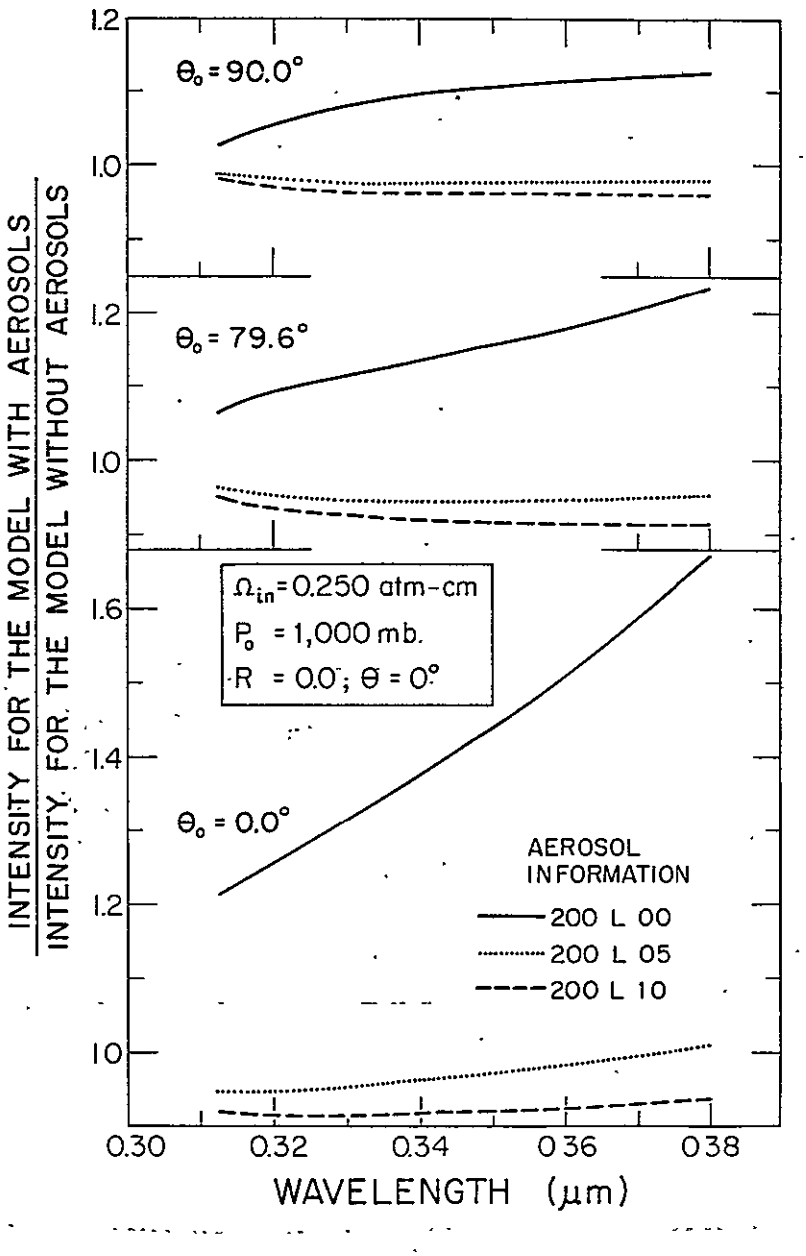

Fig. 7. Variations, as a function of the wavelength (μm), of the changes in the intensity of radiation emerging along the nadir direction ($\theta = 0°$) due to the presence of tropospheric aerosols (Total amount: 200×10^6 particles; Size distribution: *Haze L*) in the atmospheric model. Ω_{in} = 0.250 atm-cm; P_0 = 1,000 mb; R = 0.0. Solid curve: m = 1.5 - 0.0i; Dotted curve: m = 1.5 - 0.05i; Broken curve: m = 1.5 - 0.10i.

the ground, its presence results in a pseudo-wavelength dependence of the surface reflectivity. This pseudo-wavelength dependence of R cannot be corrected by the SITC4 procedure, but can be very-well corrected by the SITD1 procedure (see Sec. 1.3).

It is interesting to note that the value of total ozone estimated with the SITC4 procedure in the presence of tropospheric aerosols, is also dependent upon the wavelength pair used. As for example, values of Ω_e' as obtained with the measurements at the first and the second wavelength pairs are 0.259 and 0.273 atm-cm, respectively for the R = 0.8, $\theta_0 = 0°$ case of the 0 - 200 L 10 model.

In Table XXV, we have tabulated values of the *deviation* Δ' in the format and for the parameters of Table XXIV, but for $\Omega_{in} = 0.450$ atm-cm. The main finding from the intercomparison of the results in these two tables, is the inability of the SITD1 procedure to correct fully for the pseudo-wavelength dependence of R introduced by the tropospheric aerosols at moderate values of Ω_{in}. We even come across cases where a use of the SITD1 procedure provides results of poorer quality than those given by the SITC4 procedure. As for example, for the case R = 0.8, $\theta_0 = 84.7°$ of the model 0 - 200 L 05, we find that Δ' as obtained with the SITC4 and SITD1 procedures carries a value of -1 and -4 units, respectively.

4.6 *Combined Effect:* In this section, we propose to discuss the changes in the values of the *improved best ozone estimate* (Ω_e') when stratospheric as well as tropospheric aerosols are present in the models. Values of

C-7

TABLE XXV. Values of the *deviation* Δ' [$= 1{,}000 \times (\Omega_e' - \Omega_{in})$] for the atmospheric models with $\Omega_{in} = 0.450$ atm-cm and tropospheric aerosols; $P_0 = 1{,}000$ mb; R = 0.8.

Aerosols	Δ' for θ_0 =									
	0.0	45.0	60.0	70.0	75.6	79.6	82.5	84.7	86.7	90.0
Procedure: SITC4										
0 – 0	0	0	0	0	0	0	0	0	0	0
0 – 40 L 00	0	0	0	0	0	0	0	-1	-1	-1
0 – 200 L 00	0	0	0	0	0	0	-2	-2	-3	-5
0 – 40 L 05	1	1	0	0	-1	-1	-1	-1	-1	0
0 – 200 L 05	6	4	2	0	-1	-3	-1	-1	0	14
0 – 40 L 10	1	0	0	-1	-1	-1	-2	-2	-2	-1
0 – 200 L 10	6	4	2	0	-2	-3	-1	-2	-1	15
Procedure: SITD1										
0 – 0	0	0	0	0	0	0	0	0	0	0
0 – 40 L 00	-1	0	0	0	0	0	0	0	0	-1
0 – 200 L 00	-2	1	1	0	0	0	0	0	0	1
0 – 40 L 05	-2	-1	-1	-1	-1	-1	-1	-2	-3	-4
0 – 200 L 05	-3	-1	-1	-1	-2	-3	-3	-4	-6	-8
0 – 40 L 10	-2	-1	-1	-1	-1	-1	-1	-2	-3	-5
0 – 200 L 10	-3	-1	-1	-1	-2	-3	-3	-4	-6	-9

the *deviation* Δ' for seven different atmospheric models as obtained with the SITC4 (upper part of the table) and the SITD1 (lower part) procedures are given for the models with Ω_{in} = 0.250 atm-cm and 0.450 atm-cm in Tables XXVI and XXVII, respectively. These results are for the 1,000 mb models resting on a perfectly-absorbing surface (R = 0.0). Each part of the table contains seven rows with each row giving values of Δ' for 10 different values of θ_0, but for a selected atmospheric model. Results presented in the first row of the upper or the lower part of a table are for the models with no aerosols.

Models selected for the purpose of discussion in this section are those with very large amounts of partly-absorbing aerosols. The second, third, and the fourth rows of a part of a given table contain values of Δ' for the models 20 H 05 - 0, 0 - 200 L 05, and 20 H 05 - 200 L 05, respectively. Similarly, values of Δ' for the models 20 H 10 - 0, 0 - 200 L 10, and 20 H 10 - 200 L 10 are given in the fifth, sixth, and the seventh row, respectively.

On comparison of the algebraic sum of the values of Δ' for the models with stratospheric aerosols (20 H mm - 0) and tropospheric aerosols (0 - 200 L mm) for a given case, with the corresponding value of the models with both kinds of aerosols (20 H mm - 200 L mm), we find that the effects of these two kinds of aerosols on Ω_e' are generally additive. As for example, for the case $\theta_0 = 70°$, values of Δ' as obtained with the SITC4 procedure are 4, 3, and 8 units for the models 20 H 10 - 0, 0 - 200 L 10, and 20 H 10 - 200 L 10, respectively, when Ω_{in} = 0.250 atm-cm (see Table

TABLE XXVI. Values of the *deviation* Δ' [$= 1{,}000 \times (\Omega_e' - \Omega_{in})$] for the atmospheric models with $\Omega_{in} = 0.250$ atm-cm and stratospheric as well as tropospheric aerosols; $P_0 = 1{,}000$ mb; R = 0.0.

Aerosols	Δ' for θ_0 =									
	0.0	45.0	60.0	70.0	75.6	79.6	82.5	84.7	86.7	90.0
Procedure: SITC4										
0 - 0	0	0	0	0	0	0	0	0	0	0
20 H 05 - 0	3	3	3	3	3	1	4	0	-7	-51
0 - 200 L 05	7	6	5	3	2	1	3	2	2	11
20 H 05 - 200 L 05	10	9	8	6	5	2	7	3	-5	-
20 H 10 - 0	4	4	4	4	4	2	6	2	-7	-
0 - 200 L 10	8	7	5	3	2	1	3	2	3	13
20 H 10 - 200 L 10	12	11	10	8	6	3	10	5	-4	-
Procedure: SITD1										
0 - 0	0	0	0	0	0	0	0	0	0	0
20 H 05 - 0	1	1	1	1	1	-1	-1	-5	-13	-84
0 - 200 L 05	1	1	1	0	0	0	0	0	0	-1
20 H 05 - 200 L 05	3	3	2	2	1	-1	-1	-5	-13	-85
20 H 10 - 0	2	2	2	2	1	0	-1	-5	-13	-89
0 - 200 L 10	2	1	1	0	0	0	0	0	0	0
20 H 10 - 200 L 10	4	3	3	2	2	0	-1	-5	-14	-90

TABLE XXVII. Values of the *deviation* Δ' $[= 1{,}000 \times (\Omega_e' - \Omega_{in})]$ for the atmospheric models with Ω_{in} = 0.450 atm-cm and stratospheric as well as tropospheric aerosols; P_0 = 1,000 mb; R = 0.0.

Aerosols	Δ' for θ_0 =									
	0.0	45.0	60.0	70.0	75.6	79.6	82.5	84.7	86.7	90.0
Procedure: SITC4										
0 - 0	0	0	0	0	0	0	0	0	0	0
20 H 05 - 0	4	4	3	1	-5	-17	-7	-	-	-
0 - 200 L 05	6	5	3	1	-1	-3	2	2	5	-
20 H 05 - 200 L 05	9	8	6	2	-6	8	-4	-	-	-
20 H 10 - 0	5	5	5	4	-1	-12	-1	-	-	-
0 - 200 L 10	7	5	3	1	-1	-3	2	2	5	-
20 H 10 - 200 L 10	12	10	8	5	-3	-	-	-	-	-
Procedure: SITD1										
0 - 0	0	0	0	0	0	0	0	0	0	0
20 H 05 - 0	2	2	2	0	-5	-16	-16	-37	-73	-173
0 - 200 L 05	0	0	0	0	-1	-2	-2	-2	-3	-4
20 H 05 - 200 L 05	3	3	2	-1	-6	-18	-18	-40	-76	-192
20 H 10 - 0	3	3	3	2	-1	-10	-13	-34	-75	-190
0 - 200 L 10	0	0	0	0	-1	-2	-2	-3	-4	-5
20 H 10 - 200 L 10	4	4	4	2	-2	-13	-14	-37	-78	-204

The symbol "-" inplies that it was not possible to estimate a value of Ω_e' in that particular case.

XXVI). However, this is not always true, and some exceptions are clearly noticeable. As for example, the *deviation* Δ' obtained with the SITC4 procedure for the Ω_{in} = 0.450 atm-cm, θ_0 = 79.6° case of the models 20 H 05 - 0, 0 - 200 L 05, and 20 H 05 - 200 L 05 carries a value of -17, -3, and 8 units, respectively. This is because the procedure selects the first wavelength pair for the first two models, but the second wavelength pair for the third models. Another example of such an exception is the Ω_{in} = 0.450 atm-cm, θ_0 = 90° cases of Δ' values obtained with the SITD1 procedure.

It should be noted that the cases showing very significant underestimation of total ozone (large negative values of Δ') are generally discarded by the SITC4 procedure, but are retained by the SITD1 procedure.

4.7 *Effect of a Change in the Size-Distribution Function:* We will now consider the effect of changing the size-distribution function of the tropospheric aerosols from the *Haze L* to the *Haze J*, on the magnitude of the *improved best ozone estimate* (Ω_e') of the total ozone content (Ω_{in}) of an atmospheric column. Since a change in the size-distribution function leads to changes in the aerosol normal optical thicknesses (see Sec. 2.2 and 3.2), it was considered appropriate to normalize the attenuation (scattering + absorption) optical thicknesses of the models with the *Haze L* and *Haze J* functions at 0.3398 μm (see Table V) for a convenience of comparison. This normalization is achieved by changing the total number of tropospheric aerosol particles from one model to another (see Sec. 3.2).

In Table XXVIII, we have given values of the *deviation* Δ' for the atmospheric models with Ω_{in} = 0.250 atm-cm, and with the size-distribution of their tropospheric aerosols represented by the spherical polydispersion *Haze L* (top-half of the table); or *Haze J* (bottom-half). These models with a surface pressure of 1,000 mb, rest on a perfectly-absorbing surface (R = 0.0). These values of Δ' are obtained after computing corresponding values of Ω_e' with the SITC4 procedure. Results obtained with the SITD1 procedure are not discussed here as the tropospheric aerosols in this case were found to have a very significant effect on Ω_e' (see Sec. 4.5).

On comparison of the value of Δ' for a given θ_0 in the n-th row of the top-half of the table with the corresponding value of Δ' in the n-th row of the bottom-half of the table, we find that the change in size-distribution characteristics of tropospheric aerosols from that of *Haze L* to that of *Haze J*, has a small effect on Ω_e'. The highest difference in Δ' due to the aforementioned change in the size-distribution function occurs at $\theta_0 = 90°$ as we proceed from the model 0 - 200 L 05, to the model 0 - 1172 J 05. This small effect of the change in the size-distribution function of the tropospheric aerosols on Ω_e' can be due to a change in the phase function, or due to a small change in the attenuation optical thickness at wavelengths other than 0.3398 μm.

TABLE XXVIII. Values of the *deviation* Δ' [$= 1{,}000 \times (\Omega_e' - \Omega_{in})$] for the atmospheric models with $\Omega_{in} = 0.250$ atm-cm and tropospheric aerosols of *Haze L* and *Haze J* type size-distribution functions; $P_0 = 1{,}000$ mb; R = 0.0; Procedure: SITC4.

Aerosols	Δ' for θ_0 =									
	0.0	45.0	60.0	70.0	75.6	79.6	82.5	84.7	86.7	90.0
Size distribution function: *Haze L*										
0 - 40 L 00	0	0	0	0	0	0	0	0	0	0
0 - 200 L 00	-1	-1	0	0	0	0	0	0	-1	-2
0 - 40 L 05	2	2	1	1	1	0	1	1	1	3
0 - 200 L 05	7	6	5	3	2	1	3	2	2	11
0 - 40 L 10	2	2	1	1	1	0	1	1	1	3
0 - 200 L 10	8	7	5	3	2	1	3	2	3	13
Size distribution function: *Haze J*										
0 - 237 J 00	-1	-1	0	0	0	0	0	0	0	-1
0 - 1184 J 00	-4	-3	-1	0	0	0	-1	-1	-1	-3
0 - 234 J 05	1	1	1	1	0	0	1	0	0	2
0 - 1172 J 05	5	4	4	2	2	1	2	1	1	7
0 - 231 J 10	2	2	1	1	1	0	1	1	1	3
0 - 1156 J 10	7	6	5	3	2	1	3	2	2	11

V. CONCLUSION

This report deals with the investigations of the effect of atmospheric aerosols on the value of total ozone, in a column of the terrestrial atmosphere, estimated from the simulated measurements of the ultraviolet radiation back-scattered by it. For this purpose, simulated measurements for a number of models of cloudless terrestrial atmosphere are generated and analyzed by two different total-ozone estimation procedures, viz., SITC4 and SITD1. The SITC4 procedure, requiring measurements in five different spectral regions, is very similar to the one currently being used at NASA/GSFC for the analysis of the radiation data from the BUV experiment aboard the NIMBUS-IV satellite. The SITD1 procedure uses measurements at six wavelengths specified for the TOMS section of the SBUV/TOMS experiment aboard the forthcoming NIMBUS-G satellite. The main difference between these procedures is the treatment of the so-called effective albedo of the surface underlying the atmospheric column. Availability of an additional measurement in the spectral region with insignificant abosorption by ozone, permits the inclusion of the spectral dependence aspect of this albedo in the SITD1 procedure.

Investigations referred to in the preceding paragraph are performed for several values of the spectrally-independent, Lambert reflectivity of the surface underneath, and for ten different conditions of the solar illumination of the models from above.

Simulated measurements are generated and analyzed for 40 different atmospheric models derived from selected combinations of the following

parameters for their aerosols:

Three different values of the refractive index (m) of the aerosol material; m = 1.5 - 0.00i, 1.5 - 0.05i, and 1.5 - 0.10i.

Three different functions (viz., *Haze H*, *Haze J*, and *Haze L*) representing the size distribution characteristics of a unit volume of aerosols assumed to exist in the form of a spherical polydispersion.

Two different vertical profiles of aerosols which are referred to as the stratospheric and tropospheric distribution.

Three different total aerosol content for the stratospheric distribution and two different total aerosol content for the tropospheric distribution.

We find that the estimates of total ozone obtained from the analysis of the simulated measurements are very sensitive to stratospheric particulate contaminants especially if the sun is low, but the total stratospheric aerosol content and the total ozone content of the column are not low. The effect of tropospheric particulate pollution on the total ozone estimates is found to be very small in most cases. It is very desirable to carry out further investigations in the following directions if total-ozone estimates from the measurements of the ultraviolet radiation back-scattered by the earth-atmosphere system are required with a reasonable accuracy at all times.

(a) A critical literature survey for establishing the aerosol number-density vs. height profiles of the 15 - 50 km region on a global scale under average, and under specific, conditions.

(b) Comparison of the results obtained from the survey described under (a) above with the aerosol profiles used for the investigations reported in this study.

(c) Further investigations for models with characteristics (especially size-distribution function and vertical profile) of the stratospheric aerosols different from those used in this study.

(d) Development of a new generation of instruments which can provide some information about the stratospheric aerosols at the place and time of observation. Additional measurements aimed at determining the polarization characteristics of the back-scattered radiation with wavelengths smaller than 0.3 μm, are likely to be useful in the acquisition of such information.

(e) Improved total-ozone estimation procedures based on the information about the stratospheric aerosols under average conditions.

Evidently, commitment to such an extensive study can be made only after determining the degree of accuracy with which total-ozone estimates are required under various geographic and atmospheric conditions. To this effect, it should be pointed out that two additional pieces of information required for increasing the reliability of the satellite ozone data are the surface pressure and the spectral dependence of the surface reflectivity at the place and time of observation (Dave, 1976 B).

In the absence of additional studies along the directions outlined above and use thereof in the analysis of the actual data, we feel that

sufficient evidence exists for exercising due caution in acceptance of the BUV total-ozone estimates at their face values, especially if the conditions at the time of a given set of measurements correspond to that of low sun (zenith angle > 80°), and expectation of moderate to high amount of total ozone. To be more specific, it is possible that an observed decrease in the NIMBUS-BUV total ozone at moderate or high latitudes under the condition of known stratospheric particulate contaminants, is not due to a decrease in the actual total ozone content of the column, but is an artifact of the estimation procedure used.

Near future projects call for estimations of the total ozone from the analysis of the ultraviolet radiation back-scattered in directions other than that of the local nadir (e.g., SBUV/TOMS on the NIMBUS-G satellite). It is possible for a second more-careful look at the analysis of simulated measurements along the nadir direction to provide sufficient knowledge, which can be used for determining the effect of various parameters on total ozone estimates from measurements in the off-nadir directions. If not, it would be very desirable to extend the investigations described in the Technical Reports: I and II (Dave, 1976 A and B), and this final report of this Contract, to off-nadir geometry.

VI. REFERENCES

Braslau, N. and J. V. Dave, 1973: J. Appl. Meteor., *12*, 616 - 619.

Bullrich, K., 1964: Advances in Geophysics, *10*, 99 - 260.

Canosa, J. and H. R. Penafiel, 1973: J. Quant. Spectr. & Rad. Trans., *13*, 21 - 39.

Dave, J. V., 1964: Astrophys. J., *140*, 1292 - 1303.

Dave, J. V., 1972: "Development of Programs for Computing Characteristics of Ultraviolet Radiation: Technical Report—Scalar Case," Contract No. NAS5-21680, NASA Goddard Space Flight Center, Greenbelt, Maryland, Program I: 43 pp., Program II: 38 pp.

Dave, J. V., 1974: "A Direct Solution of the Spherical-Harmonics Approximation to the Transfer Equation for a Plane-Parallel Nonhomogeneous Atmosphere," Report No. UCRL-51581, Lawrence Livermore Laboratory, Livermore, California; also available through NITS, 49 pp.

Dave, J. V., 1976 A: "Investigation of the Effect of Atmospheric Dust on the Determination of Total Ozone from the Earth's Ultraviolet Reflectivity Measurements; Technical Report: I," Contract No. NAS5-23556, NASA Goddard Space Flight Center, Greenbelt, Maryland, 131 pp.

Dave, J. V., 1976 B: "Investigation of the Effect of Atmospheric Dust on the Determination of Total Ozone from the Earth's Ultraviolet Reflectivity Measurements; Technical Report: II," Contract No.

NAS5-23556, NASA Goddard Space Flight Center, Greenbelt, Maryland, 128 pp.

Dave, J. V. and B. H. Armstrong, 1974: J. Atmos. Sci., *31*, 1934 - 1937.

Dave, J. V. and J. M. Canosa, 1974: J. Atmos. Sci., *31*, 1089 - 1101.

Dave, J. V. and C. L. Mateer, 1967: J. Atmos. Sci., *24*, 414 - 427.

Dave, J. V. and C. L. Mateer, 1968: J. Geophys. Res., *73*, 6897 - 6913.

Deirmendjian, D., 1969: *Electromagnetic Scattering on Spherical Polydispersions*, Elsevier, New York, 290 pp.

Mateer, C. L., D. F. Heath and A. J. Krueger, 1971: J. Atmos. Sci., *28*, 1307 - 1311.

Mie, G., 1908: Ann. Physik, *25*, 377 - 445.